Analysis of an Anti-vibration Glove for Vibration Suppression of a Steering Wheel

Oreoluwa A. Alabi

Thesis submitted to the Faculty of the
Virginia Polytechnic Institute and State University
in partial fulfillment of the requirements for the degree of

Master of Science
in
Mechanical Engineering

Oumar R. Barry, Chair
Michael L. Madigan
Lei Zuo

December 9, 2021
Blacksburg, Virginia

Keywords: Vibration Isolation, Multi-objective Optimization, Anti-vibration Gloves
Copyright 2021, Oreoluwa A. Alabi

Analysis of an Anti-vibration Glove for Vibration Suppression of a Steering Wheel

Oreoluwa A. Alabi

(ABSTRACT)

Exposure to severe levels of hand-arm vibration can lead to hand-arm vibration syndrome. Towards curbing the development of hand-arm vibration syndrome, studies have shown that anti-vibration gloves effectively reduce the transmission of unwanted vibration from vibrating equipment to the human hand. However, most of these studies have focused on the study of anti-vibration gloves for power tools such as chipping hammers, and not much work has been done to design anti-vibration gloves for steering wheels. Also, as most of these studies are based on experimental or modeling techniques, the level of effectiveness and optimum glove properties for better performance remains unclear. To fill this gap, the dynamics of the hand-arm system, with and without gloves, coupled to a steering wheel is studied analytically in this work. A lumped parameter model of the hand-arm system with hand-tool interaction is modeled as a linear spring-damper system. The model is validated by comparing transmissibility obtained numerically to transmissibility obtained from experiments. The resulting governing equations of motion are solved analytically using the method of undetermined coefficients. Parametric analysis is performed on the bio-mechanical model of the hand-arm system with and without a glove to identify key design parameters. It is observed that the effect of glove parameters on its performance varies based on the frequency range. This observation further motivates us to optimize the glove parameters, using multi-objective optimization, to minimize the overall transmissibility in different frequency ranges.

Analysis of an Anti-vibration Glove for Vibration Suppression of a Steering Wheel

Oreoluwa A. Alabi

(GENERAL AUDIENCE ABSTRACT)

When the human hand is exposed for a long time to vibrations generated from hand-held tools, such as Jack-hammers, rock breakers and chipping hammers, humans are in danger of developing hand-arm vibration syndrome. Hand-arm vibration syndrome is dangerous as severe episodes of this syndrome could lead to gangrene and eventually amputation of the fingers. To prevent the occurrence of hand-arm vibration syndrome, some researchers have explored the effectiveness of anti-vibration gloves through experiments. However, no work has been performed to identify the optimal glove design that best optimizes an anti-vibration glove for steering wheel applications. To address this issue, this thesis studied a mathematical model of the human-hand, wearing an anti-vibration glove attached to a steering wheel system. To ensure this model could successfully replicate real life applications, measurements computed with the model were compared with measurements on the human-hand obtained from experiments. After successfully ensuring that the model closely replicated real-life measurements, the model was used to design an Anti-vibration glove with optimal values to protect the hand from hand-arm vibration syndrome.

Dedication

To my parent Adesola and Modupe.

Acknowledgments

I would like to thank my parents for their encouragement, love and support. I would also like to thank my advisor, Dr. Barry, for providing me with the opportunity to work on this research topic. His guidance and constant encouragement was invaluable in completing this work. I am grateful for my committee members Dr. Michael Madigan and Dr. Lei Zuo. I am also grateful to Dr. Sunit Kumar Gupta for his advice and collaboration on different aspects of this work.

Contents

List of Figures

List of Tables

List of Abbreviations

AV Anti-vibration

DOF Degree of Freedom

EPS Electric Power Steering system

HAS Hand Arm System

HAVS Hand-Arm Vibration Syndrome

VWF Vibration White Finger

Chapter 1

Introduction

1.1 Motivation

This thesis was written to improve the mitigation of hand-arm vibrations transmitted from a steering column through the study and optimization of a passive isolation device, an anti-vibration glove. Hand-arm vibration (HAV) can be defined as vibrations transferred from tools, such as electric grass trimmers and steering wheels, to the human hands. Numerous studies have revealed that HAV can lead to the occurrence of hand-arm vibration syndrome (HAVS) [42].

HAVS is a condition that consists of neurological, vascular and, musculoskeletal symptoms [7, 18, 35, 79]. The symptoms of HAVS are initially intermittent but when left uncontrolled can become continuous [43]. Some of the neurological symptoms of HAVS include tingling, paraesthesia, sensory loss and decreased dexterity. These symptoms tend to be worse in the dominant hand [24]. Damages to the muscle and nerve supply of the human hand may also occur leading to the loss of grip strength at the hand [63]. It has also been observed that injuries that cause structural changes to nerves surrounding the wrist may occur [76].

The vascular symptoms of HAVS are predominantly apparent through the narrowing of the arteries of the fingers. This occurence is mainly known as vibration white finger (VWF). In the earlier stages of HAVS, the tips of the human fingers may blanch upon exposure to

(a) Vibration-induced white finger

(b) Vibration-induced white finger

Figure 1.1: Episodes of vibration white finger on the human hand [57]

.

a cold environment. An episode of blanching of the human hand is shown in Figure1.1 As the disease progresses, the frequency duration and severity of blanching also progresses [43]. Musculoskeletal complications due to HAVS involve osteoporosis of the wrist, elbow and acromi-oclavicular joint following prolonged vibration exposure [38]. HAVS can result in loss of blood supply in the fingers leading to gangrene and eventually amputation [82]. Other symptoms of HAV include pain in the hand-arm, carpal tunnel syndrome, paresthesisia, hyperhidrosis, ulnar neuropathy, and soft tissue wasting [58]. Apart from the physical discomfort accruing to HAVS, there is also a hefty monetary cost for the treatment of the

symptoms of HAVS [42].

The onset of HAVS must be eliminated due to the debilitating effects described above and also due to its wide spread nature. Some of the workers exposed to HAV include those in the mining industry [44, 58, 75], agricultural industry [15, 74, 89] as well as the military [1]. This is a huge concern as it is estimated that more than four million workers are exposed to HAV and 50% of them will develop symptoms associated with HAVS [80].

Most of the work done on studying and reducing HAV focuses on vibrations stemming from powerhand tools [9, 10, 18, 28, 35, 41, 58, 64]. However, there is little work on studying and attenuating vibrations transmitted from steering wheels of heavy equipment vehicles (HEV) such as haul trucks and wheel dozers. Regarding highlighting the harmful vibration exposure from steering wheels, Goglia *et al.* conducted experimental measurements on a small four-wheel drive tractor and revealed that 10 % of drivers exposed to steering wheel vibrations can have white fingers in less than 2 years [31, 32]. This is because their predicted daily exposure to vibrations was found to be about six times higher than the maximum daily exposure action value recommended by the European Council Directive 2002/44EC.

Due to the risk posed when the HAS is exposed to vibrations from a steering wheel, and since none of the works in literature have systematically analyzed the optimum values of the anti-vibration glove material properties [22, 60, 67, 82], this thesis will focus on the development of an optimum anti-vibration glove for steering wheel applications. This task will be achieved by studying a model of the hand-arm, anti-vibration glove and steering column to determine what properties of the passive isolation device best attenuate vibrations.

1.2 List of Contributions

The contributions of this thesis are summarized below:

1. A review of the debilitating conditions which can arise due to the prolonged exposure of the human hand to vibrations. This review is used to highlight the need for the development of devices that reduce the amount of vibrations transferred to the human hand.

2. A review of the nature of vibrations transmitted to the HAS from a steering wheel. It is important that the level of vibrations transmitted to the hand is quantified so that vibration reducing devices, such as AV gloves, can be developed appropriately to reduce vibrations transmitted to the hand.

3. A review on models of a steering wheel, HAS and AV glove that describe vibration transmissibility. This review helps to identify models of the HAS, AV glove and steering wheel that can be studied to pick AV glove parameters that reduce vibrations.

4. Experimental validation of a model of a gloved HAS coupled to a base excited steering wheel.

5. Development of an analytical solution for a model of the coupled gloved HAS and steering wheel.

6. A parametric study and optimization of the parameters of an AV glove using the multi-objective optimization algorithm.

1.3 Thesis Structure

The remainder of the thesis is structured as follows:

Chapter 2 presents a literature review summarizing the selection of a hand-arm system, AV glove and steering wheel model.

Chapter 3 presents the model studied to select key design parameters for the Anti-vibration glove. The model of a gloved hand-arm coupled to a steering wheel is validated using experimental measurements, and an analytical solution for the model is presented.

Chapter 4 outlines the numerical verification of the analytical solution for the system. Afterward, a parametric study using the analytical solution is performed to identify key design parameters of the Anti-vibration glove.

Chapter 5 presents the optimal parameters for the Anti-vibration glove that are obtained using the multi-objective optimization scheme.

Chapter 6 concludes the thesis with a summary of the work undertaken in the thesis and future work.

1.4 Selected Publications

Disclaimer: Content from the following publications are used throughout this work.

Conference Proceedings

(a) Gupta, S. K., **Alabi, O.**, Kakou, P. C., & Barry, O. (2019, October). On the Modeling and Optimization of Anti-Vibration Gloves for Hand-Arm Vibration Control. In Dynamic Systems and Control Conference (Vol. 59155, p. V002T27A007). American Society of Mechanical Engineers.

Journal Publications

(b) **Alabi, O.**, Gupta, S. K., & Barry, O. (2021). Theoretical Analysis and Optimization of a Gloved Hand–Arm System. Journal of Biomechanical Engineering, 143(9), 091009.

Chapter 2

Literature Review

2.1 Steering System

To attenuate vibrations transmitted from the steering wheel of a vehicle to the hand, it is important to determine how vibrations are transmitted from various parts of a vehicle to the steering wheel. It is also essential to quantify the vibrations transmitted to the steering wheel. As such, a review of causes of vibrations to a steering wheel system is presented. Also, an overview of methods to model the steering wheel systems is done.

It has been reported that the vibration level at a steering wheel depends on some factors such as the road surface on which a vehicle is driven, the dynamic nature of the vehicle's tyres, engine, suspension system design and steering mechanism [29]. Dynamic instability of a vehicle's engine and steering rods have also been identified as key factors which affect the vibration level transmitted to a steering wheel [78]. These factors produce different patterns of vibrations, which are transmitted from the steering rod of the vehicle to the steering wheel [1]. These different patterns of vibration which vary in magnitude, frequency and direction, elicit different responses from the HAS. As such, it is important to quantify some of their patterns, such as the direction in which vibrations are transmitted to the hand-arm.

According to the ISO standard 5349-1 [49], the different directions vibrations can be transmitted to the HAS include the three orthogonal directions,*i.e,* the x, y and z directions.

Various reports from literature have revealed how the dominant axis of vibrations transmitted to a steering wheel varies with driving conditions. Such examples include a study by Tewari *et al.* which revealed that the root mean square(rms) vibration acceleration transmitted to the hands from a hand tractor was highest in the x-axis when used for transportation, rota-tilling and rota-puddling [78]. When Yoo *et al.* evaluated the vibrations at a steering wheel while driving on roads of different types, their results revealed that the rms vibration acceleration was higher in the x-axis for roads such as an asphalt road [87]. While driving on other roads such as a Belgian roads produced higher rms acceleration values in the y-axis. This research work also showed that a higher vehicle speed could result in a higher or lower rms vibration acceleration depending on the road the vehicle was being driven on. A study by Aziz *et al.* on a three-tonne truck showed that when driving on a main road, the dominant vibration frequency component is in the z-axis [5]. Goglia *et al.* studied vibrations emitted to the steering wheels of a four-wheel tractor and realized that the dominant acceleration, when the tractor was in idle and full load operating conditions, were transmitted in the z-axis [31]. From most of these studies highlighted, it is evident that vibrations at the steering wheel were experienced in one direction. As such, the direction of vibration transmission in this study will be assumed to be in one axis.

Also, to determine the vibration transmitted from the steering system to the hand, it is paramount that a model which predicts how vibrations are transmitted through the steering wheel is selected and studied. Towards achieving this aim, we highlight previous attempts to create models to study the dynamics, including vibration transmission, of the steering wheel system. In [90], the hydrostatic steering system of an agricultural tractor was studied by modelling it as a lumped parameter model. With this model, the effect of the steering wheel's design parameters on a driver's effort during steering, and steering wheel torque was discussed. Towards investigating the influences of a vehicle's steering wheel system

parameters on the on-center handling performance of a vehicle, Sun *et al.* studied a model of an hydraulic steering system and a vehicle multibody system [77]. Zhang *et al.* developed a nonlinear model of a hydraulic steering wheel system and employed free and forced vibration analysis to determine critical design elements of their system [91]. To reduce pressure ripples generated in an electric power steering system (EPS), Li *et al.* described the dynamics of the EPS system using a Takagi-Sugeno (T-S) fuzzy model. Then, they evaluated the ability of a fuzzy controller to reduce the pressure ripples generated by the EPS model [55]. Li *et al* also investigated the application of robust and nonlinear sliding mode control to reduce torque ripple in a steering system which was introduced as a nonlinear state-space model [54]. More recently, Li and Shim investigated the steering feel response of a column power assist steering wheel system (CEPAS) by running simulations on a mechanical model of the CEPAS [56]. Using a lumped parameter steering system model, Lee *et al.* developed a torque feedback control algorithm to overcome the trade-off between steering feel and stability [53].

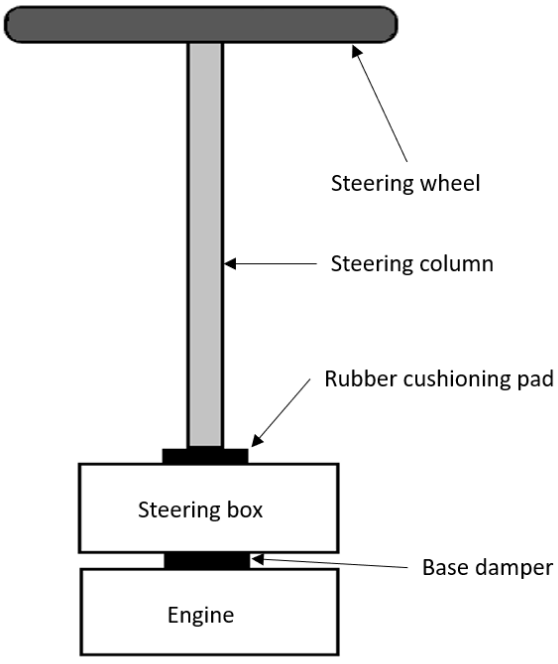

Figure 2.1: Schematic showing components on an electric power steering wheel system.

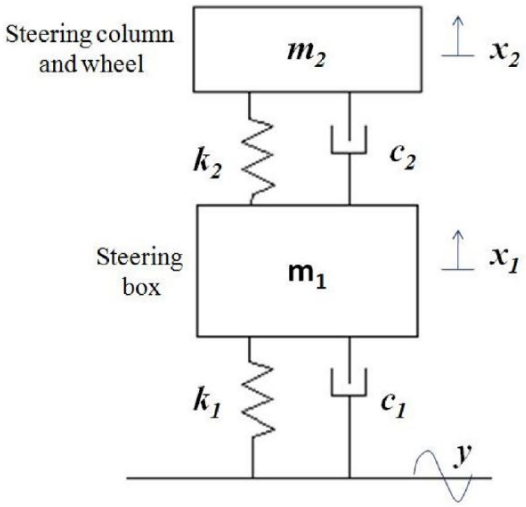

Figure 2.2: Steering wheel system studied by Sakthivel *et al.* [74] .

In a bid to study methods to reduce vibrations transmitted to the steering wheel of an agricultural tractor, Saktivel *et al.* studied a model of a steering system equipped with radial and axial damper components [74]. The 2-DOF model of the steering system consisted of the steering column and wheel components which were described as a lumped mass as seen in Fig. 2.2. With this model, Saktivel *et al.* were able to accurately predict measured vibrations at the steering wheel obtained from experiments. To improve this model, Freund *et al.* modelled the steering column as a continuous system [26] to help understand the cantilever effect of the steering column. Towards understanding how vibrations affect the hand-arm, this work will take a different approach by modelling the steering wheel system as a single degree of freedom consisting of a steering wheel, steering column and a rubber cushioning pad. For visualization of how these components are arranged in a typical steering system, a schematic is presented in Fig. 2.1. In the next section, a review concerning HAS and AV gloves is presented.

2.2 Hand-arm system Models

One of the most common ways to understand the effect of vibrations on the HAS is to study biomechanical models of the HAS [16, 19]. In order to develop these models so that they accurately represent the experimentally measured responses of the hand-arm, the models are built with an intent to characterize the complex bio-dynamic responses of the HAS [13, 16, 19, 36, 37, 69]. It is important that the biodynamic responses of the HAS are understood so that phenomena associated with HAVS can be interpreted [18, 33, 84]. Some commonly known bio-dynamic responses of the HAS include its vibration amplitude, vibration transmissibility, mechanical impedance and vibration power absorption.

Previous attempts at studying models of the HAS include the research performed by Rakheja *et al.* [70]. In this work, Rakheja *et al.* evaluated the ability of 12 HAS models to function as a mechanical simulator which could help predict the hand's response to vibrations from power tools. However, it was discovered that the majority of these models were not adequate to serve as mechanical simulators. The reason was that the models did not produce either ideal mechanical impedance or static deflection values. In order to develop models which could be used to evaluate risks due to vibration exposure, Adewusi *et al.* suggested that anatomically analog models of the hand-arm be developed on the basis of mechanical impedance and vibration transmissibility [2]. Towards generating anatomically analog models of the HAS, Cherian *et al.* proposed a model of the HAS wherein the tissue/muscle and bones of the forearm and upper-arm were represented by lumped masses, coupled to the elbow and shoulder joints via visco-elastic properties. The hand was represented as a lumped mass coupled to the forearm mass by the visco-elastic representation of the wrist joint. After obtaining the model parameters, via vibration transmissibility measurements, it was revealed that the model output did not agree with measured data [13]. Another attempt at developing an anatomically structured model was made by Fritz *et al.*. The model had

the same HAS anatomy employed by Cherian *et al.*. However, they obtained the model parameters using driving point data. This model results also did not agree with experimentally measured results [27].

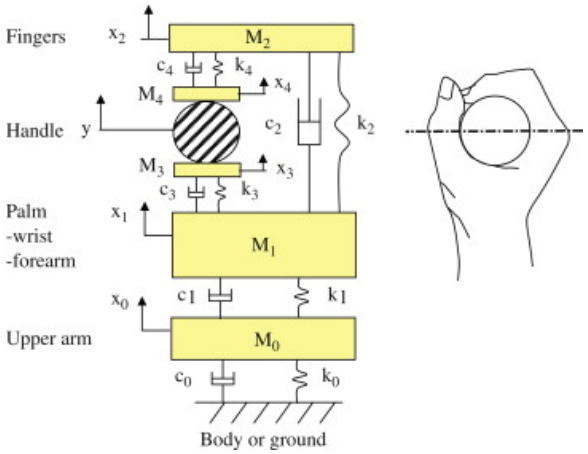

Figure 2.3: HAS model as a clamp-like structure [20]

Dong *et al.* proposed a HAS model wherein the hand was represented, as a clamp-like structure as shown in Figure 2.3 [16, 19]. The tissue/muscle/skin and bones of the palm-wrist forearm structure and the fingers were represented as separate lumped masses. These masses were both coupled to the handle, from which vibration is generated, via visco-elastic elements. The model parameters were obtained using mechanical impedance data, and it was reported that the measured and model impedance responses matched. Given the difference in the dynamic properties of the finger and palm of the human hand-arm, it is preferable that a model which can provide insight on the effect of vibrations on the finger and palm-wrist structures separately is studied. As such, we employ the model developed my Dong *et al.* to understand the how vibrations transmitted from a steering wheel affect the HAS.

2.3 Design of Anti-vibration gloves

One of the passive isolation devices employed to minimize HAV is an AV glove. AV gloves act as a cushion or suspension system between the tool and the hand [20]. AV gloves are often employed because they are a convenient means by which vibration levels can be reduced [30, 34, 71, 75]. AV gloves are commonly made of air-bubble, gel and hybrid combinations of visco-elastic materials [39, 40, 61, 73]. Different studies on AV gloves have revealed that they can amplify or reduce vibration transmissibility at the hand depending on their material and geometry properties [12, 23, 44, 45, 86]. Also, the effectiveness of AV gloves differs from one application to another [20, 22, 60, 67, 82].

To assess the effectiveness of AV gloves in isolating vibrations from hand tools, a metric that describes the ratio of the vibration at the glove-hand interface to the handle vibration is often used [20]. The metric is referred to as vibration transmissibility. Using vibration transmissibility, the International Organisation of Standardization has set a standard that helps determine if a glove offers enough vibration protection to be characterized as an AV glove [25]. According to this standard, a glove can be characterized as an AV glove when the frequency-weighted palm acceleration transmissibility in the medium(25-200Hz) and high (200-1250Hz) frequency ranges are $\leqslant$ 0.9 and 0.6 respectively. Also, the standard dictates that an AV glove have the same vibration-reducing material and thickness as used at the palm. Towards evaluating the effectiveness of some AV gloves, Welcome *et al.*, experimentally determined the effectiveness of a gel-filled and an air bladder AV glove [82]. Using an adapter, equipped with a miniature tri-axial accelerometer between the hand and the glove material, Welcome *et al.* were able to measure the vibration transmissibility of AV gloves. By measuring the vibrations on the hand with and without an AV glove, other researchers have been able to determine the vibration transmissibility of AV gloves [11, 65]. Also, by

predicting the vibrations on the hand with and without a glove using a model of the HAS and AV glove, Dong *et al.* [20] have been able to determine the vibration transmissibility of AV gloves. Using the same approach as employed by Dong, this thesis will analyze and optimize the parameters of an AV glove in order to provide the smallest vibration transmissibility possible.

Researchers have employed AV gloves to isolate vibrations generated by hand tools such as impact rock drills and jackhammers [8, 39, 40]. However, these AV gloves may not effectively isolate steering wheel vibrations due to the difference in the dynamics of the steering wheel and hand tools. This is so because the dynamics, such as the resonance frequency of different vibrating equipments may vary. As such, the vibrations transmitted to the palm and finger substructures of the HAS will also vary. Previous research shows that vibrations generated from different tools can be transmitted to different parts of the HAS and may cause various problems at different locations [17, 46, 66, 68, 72]. As such, this thesis will analyze and determine the properties of an AV glove needed to reduce vibrations from a steering wheel, as the AV gloves proposed for hand tools may not be effective at the steering wheel.

Works in Literature have explained that due to the different biodynamic properties at the palm and finger, the same glove material used at the palm may not effectively attenuate vibrations at the fingers [21, 45]. To solve this problem, this thesis proposes that the multi-objective optimization scheme be employed to select glove materials that can effectively reduce vibrations at the palm and finger side of the HAS. Some background on multi-objective optimization is presented in the next section.

2.4 Multi-objective Optimization

Multi-objective optimization is employed for design problems that have more than one objective function which needs to be optimized. Due to the conflicting nature of design parameters to be optimized, it may not be possible to employ single objective optimization to optimize a vector of design objectives. As such, multi-objective optimization is often employed [6]. A multi-objective optimization scheme concerning the minimization of objective functions $F(X)$, subject to constraints, is often presented as:

$$\begin{cases} \text{Minimize } F(X) \\ \text{subject to g(X)} \leq 0 \\ where\ X = [X_1, X_2, ..., X_k]^T \\ F(X) = [F_1(X), F_2(X), ..., F_q(X)]^T \\ g(X) = [g_1(X), g_2(X), ..., g_m(X)]^T \end{cases} \tag{2.1}$$

where q is the number of objective functions, m is the number of inequality constraints and k is the number of independent design variables. Due to the conflicting nature of the objective functions to be optimized, the multi-objective algorithm provides a set of solutions rather than a unique solution. Unlike a single objective optimization problem where the optimal solution is unique, a single solution hardly satisfies multiple objectives simultaneously. As such, a multi-objective optimization scheme yields a set of trade-off solutions. These set of solutions are referred to as non-inferior solutions [88]. This concept of non-inferiority is also known as Pareto optimality [85]. The solutions obtained from a multi-objective optimization are Pareto optimal because they are the best solution candidates compared to other solutions in the design space. They are non-inferior because no objective function amongst the Pareto solutions can be improved without detriment to the other objective

function [4]. An illustration of this concept is shown in Fig. 2.4, where the Pareto optimal solutions lie on the curve where A, B and C are marked.

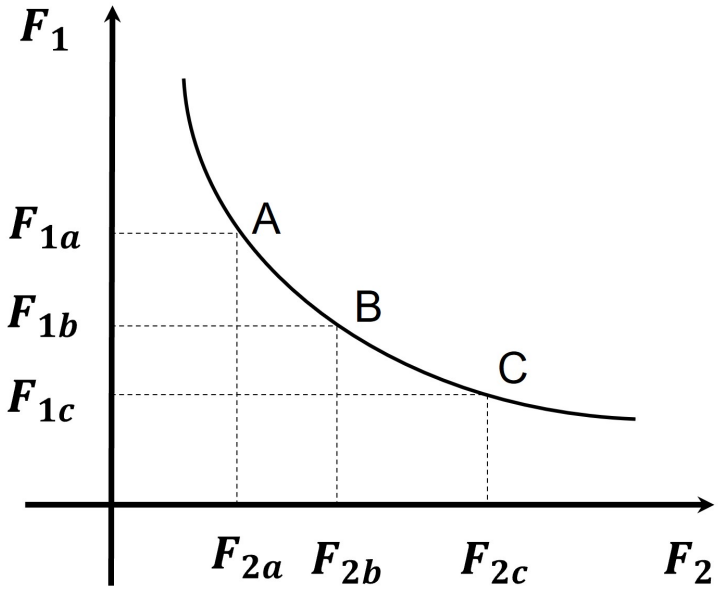

Figure 2.4: Illustration showing Pareto-optimal solutions for two objective function.

A, B and C are non-inferior solutions as an improvement (smaller objective function value) in F_1 or F_2 will lead to degraded performance in F_2 or F_1 respectively.

Multi-objective optimization has been employed in works encompassing design for engine optimization [14, 92] as well as design of vibration isolators in structural design problems [52, 59, 62, 81].

Chapter 3

Development of Analytical solution for Gloved Hand-arm System

3.1 Mathematical Modelling

The schematics of a MDOF model of the hand-arm system, without and with gloves, are shown in Fig. 3.1. Both HAS models were originally developed by Dong *et al.* [20]. This model is an extension of the MDOF model studied in[20]. The schematic of the hand-arm system without an AV glove is shown in Fig. 3.1(a). In this model, the hand is represented by a clamp-like structure with m_f and m_p representing the masses of the fingers and combined palm and wrist bone structures, respectively. m_f and m_p are connected through linear viscous and spring elements (c_1, k_1), representing the visco-elastic properties of carpal and metacarpal bones. The masses of tissues and skin covering the fingers and palm-wrist, which is further in contact with the handle of vibrating equipment, are represented by m_{tf} and m_{tp}, respectively. The tissue masses of the fingers and palm-wrist, i.e., m_{tf} and m_{tp}, are coupled to m_f and m_p, respectively through linear viscous and spring elements (c_2, k_2) and (c_3, k_3) as shown in Fig. 3.1. The mass of the bones, tissues, and the skin of the forearm and upper arm are represented by the lumped mass m_0. Also, the linear viscous-elastic properties of the forearm and upper arm are lumped at the wrist (c_w, k_w). The body/trunk is modeled as a fixed surface and connected to mass m_0 through linear spring and viscous elements

(c_0 and k_0). The vibrating equipment considered here is a steering wheel connected to the steering box via a steering column [26, 74]. In the current work, vibrations transmitted to the steering box via the engine are modeled as external excitation. Considering the steering column as a rigid bar with a very high stiffness, the visco-elastic properties of the steering column are ignored. Instead, the connection between the steering wheel and steering box is taken to be the visco-elastic property of a rubber cushioning pad between the steering column base and steering box. The handle of the vibrating equipment is modeled as lumped mass m_H, which is in contact with the fingers and palm-wrist. The rubber cushioning pad connecting the handle and the base(which is excited) is modeled with equivalent linear spring (k_s) and viscous damper (c_s). The value of m_H is obtained from [26] while the values for (k_s) and (c_s) are estimated.

The schematic of the hand-arm system with an AV glove has been shown separately in Fig. 3.1(b). The glove material between the handle and gloved-hand interface is represented by linear viscous (c_6, c_7) and spring elements (k_6, k_7) with lumped mass elements (m_{g3}, m_{g4}, m_{g5}, m_{g6}) distributed at the fingers and palm-side interface. The other side of the glove is represented by the additional masses (m_{g1} and m_{g2}) with linear viscous damper (c_4) and stiffness (k_4) as shown in Fig. 3.1b. Note that the remaining parameters for this model are the same as the hand-arm system without gloves.

For this analytical model, $z(t)$ is the external excitation. The other generalized coordinates of the hand-arm system with a glove are chosen as the motion of the finger tissue and skin mass m_{tf} (z_{tf}), palm-wrist tissue and skin mass m_{tp} (z_{tp}), fingers mass m_f (z_f), palm-wrist mass m_p (z_p), handle mass m_H (z_H) and lumped fore-arm and upper-arm mass m_0 (z_0) along the $z-$ direction, making it a 6-DOF system. However, it should be noted that for the case of the hand-arm system without a glove z_{tf} and z_{tp} will be the same as z_H; which further makes it a 4-DOF model. Having established all the generalized coordinates, we now use

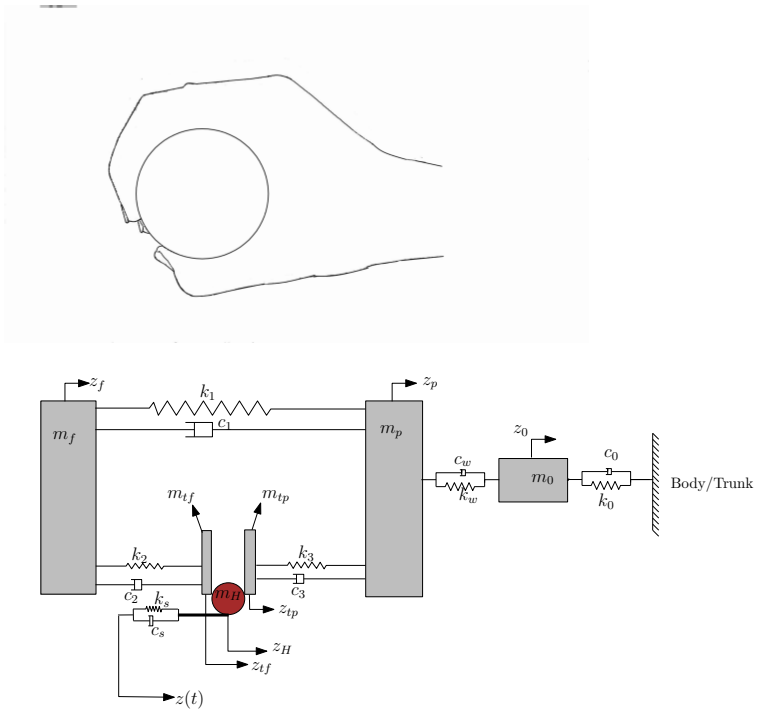

(a)

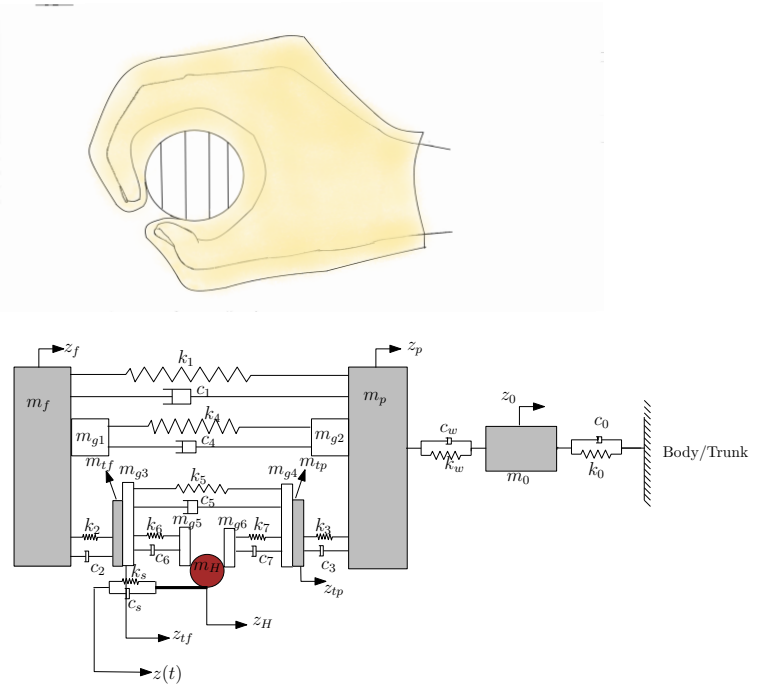

(b)

Figure 3.1: Schematic of hand-arm system (a) without glove, and (b) with glove coupled to a steering wheel [20].

the energy method to obtain the equations governing the dynamics for both scenarios.

Case 1: For the case of the hand-arm system without a glove (Fig. 3.1a) the total kinetic energy (T) and the potential energy (U) of the system are given by

$$T = \frac{1}{2}m_0\dot{z}_0^2 + \frac{1}{2}m_p\dot{z}_p^2 + \frac{1}{2}m_f\dot{z}_f^2 + \frac{1}{2}\left(m_{tp} + m_{tf} + m_H\right)\dot{z}_H^2\,, \tag{3.1a}$$

$$\begin{aligned} U = {} & \frac{1}{2}k_0 z_0^2 + \frac{1}{2}k_w\left(z_0 - z_p\right)^2 + \frac{1}{2}k_1\left(z_p - z_f\right)^2 \\ & + \frac{1}{2}k_2\left(z_H - z_f\right)^2 + \frac{1}{2}k_3\left(z_p - z_H\right)^2 + \frac{1}{2}k_s\left(z_H - z\right)^2\,. \end{aligned} \tag{3.1b}$$

Accordingly, the Lagrange function for this system is defined as

$$L = T - U\,, \tag{3.2}$$

and the equations governing the dynamics of the system with time can be obtained from the Euler-Lagrange equation

$$\frac{d}{dt}\left(\frac{\partial L}{\partial \dot{z}_i}\right) - \frac{\partial L}{\partial z_i} = F_i\,, \tag{3.3}$$

where $z_i's$ are the generalized coordinates and F_i represents the force in z_i coordinate. These generalized co-ordinates for the hand-arm system without gloves are $\{\mathbf{z}\} = [z_0,\, z_f,\, z_p,\, z_H]'$. The forces in the generalized coordinates can be written as:

$$\begin{bmatrix} F_1 \\ F_2 \\ F_3 \\ F_4 \end{bmatrix} = \begin{bmatrix} -c_0\dot{z}_0 - c_w\left(\dot{z}_0 - \dot{z}_p\right) \\ -c_1\left(\dot{z}_f - \dot{z}_p\right) - c_2\left(\dot{z}_f - \dot{z}_H\right) \\ -c_w\left(\dot{z}_p - \dot{z}_0\right) - c_1\left(\dot{z}_p - \dot{z}_f\right) - c_3\left(\dot{z}_p - \dot{z}_H\right) \\ -c_2\left(\dot{z}_H - \dot{z}_f\right) - c_3\left(\dot{z}_H - \dot{z}_p\right) - c_s\dot{z}_H + k_s z + c_s\dot{z} \end{bmatrix} \tag{3.4}$$

Therefore, the equations of motion for the system in these coordinates can be obtained using Eqs. (3.1), (3.2), and (3.3), and can be written in compact form as

$$[\mathbf{M}]\{\ddot{\mathbf{z}}\} + [\mathbf{C}]\{\dot{\mathbf{z}}\} + [\mathbf{K}]\{\mathbf{z}\} = \{\mathbf{F_{eq}}\} \tag{3.5}$$

where [**M**], [**C**], and [**K**] are (4×4) inertia, damping and stiffness matrices, respectively, $\{\mathbf{F_{eq}}\}$ is (4×1) force vector and $\{\mathbf{z}\}$ is (4×1) generalized displacement coordinate vector. These matrices are defined in Appendix A. In a next step, we present the equations of motion governing the dynamics of the hand-arm system with gloves.

Case 2: The total kinetic energy and the potential energy of the hand-arm system with gloves are given as

$$T_1 = \frac{1}{2}m_0\dot{z}_0^2 + \frac{1}{2}\left(m_p + m_{g2}\right)\dot{z}_p^2 + \frac{1}{2}\left(m_f + m_{g1}\right)\dot{z}_f^2 + \frac{1}{2}\left(m_{tp} + m_{g4}\right)\dot{z}_{tp}^2 + \frac{1}{2}\left(m_{tf} + m_{g3}\right)\dot{z}_{tf}^2 + \frac{1}{2}\left(m_{g5} + m_{g6} + m_H\right)\dot{z}_H^2\,, \tag{3.6a}$$

$$U_1 = \frac{1}{2}k_0 z_0^2 + \frac{1}{2}k_w\left(z_0 - z_p\right)^2 + \frac{1}{2}k_1\left(z_p - z_f\right)^2 + \frac{1}{2}k_2\left(z_{tf} - z_f\right)^2 + \frac{1}{2}k_3\left(z_p - z_{tp}\right)^2 + \frac{1}{2}k_4\left(z_p - z_f\right)^2 + \frac{1}{2}k_5\left(z_{tp} - z_{tf}\right)^2 + \frac{1}{2}k_6\left(z_H - z_{tf}\right)^2 + \frac{1}{2}k_7\left(z_{tp} - z_H\right)^2 + \frac{1}{2}k_s\left(z_H - z\right)^2. \tag{3.6b}$$

Accordingly, the Lagrange function for this system is defined as

$$L_1 = T_1 - U_1\,, \tag{3.7}$$

and therefore, the Euler-Lagrange equation for this system will be

$$\frac{d}{dt}\left(\frac{\partial L_1}{\partial \dot{\hat{z}}_i}\right) - \frac{\partial L_1}{\partial \hat{z}_i} = \hat{F}_i\,, \tag{3.8}$$

where $\hat{z}_i$ are generalized coordinates of the system with gloves and $\hat{F}_i$ represents the force in $\hat{z}_i$ coordinate. The generalized coordinates for the hand-arm system with gloves will be $\{\hat{\mathbf{z}}\} = \left[z_0,\, z_f,\, z_p,\, z_{tp},\, z_{tf},\, z_H\right]'$. The forces in the generalized coordinates can be written as:

$$\begin{bmatrix} \hat{F}_1 \\ \hat{F}_2 \\ \hat{F}_3 \\ \hat{F}_4 \\ \hat{F}_5 \\ \hat{F}_6 \end{bmatrix} = \begin{bmatrix} -c_0\dot{z}_0 - c_w\left(\dot{z}_0 - \dot{z}_p\right) \\ -\left(c_1 + c_4\right)\left(\dot{z}_f - \dot{z}_p\right) - c_2\left(\dot{z}_f - \dot{z}_{tf}\right) \\ -\left(c_1 + c_4\right)\left(\dot{z}_p - \dot{z}_f\right) - c_3\left(\dot{z}_p - \dot{z}_{tp}\right) - c_w\left(\dot{z}_p - \dot{z}_0\right) \\ -c_5\left(\dot{z}_{tp} - \dot{z}_{tf}\right) - c_3\left(\dot{z}_{tp} - \dot{z}_p\right) - c_7\left(\dot{z}_{tp} - \dot{z}_H\right) \\ -c_5\left(\dot{z}_{tf} - \dot{z}_{tp}\right) - c_2\left(\dot{z}_{tf} - \dot{z}_f\right) - c_6\left(\dot{z}_{tf} - \dot{z}_H\right) \\ -c_6\left(\dot{z}_H - \dot{z}_{tf}\right) - c_7\left(\dot{z}_H - \dot{z}_{tp}\right) - c_s\dot{z}_H + k_s z + c_s\dot{z} \end{bmatrix} \tag{3.9}$$

Hence, the equations of motion for the hand-arm system with glove in these coordinates can be obtained using Eqs. (3.6), (3.7), and (3.8), and can be written in a compact form as

$$\left[\mathbf{M_1}\right]\left\{\ddot{\hat{\mathbf{z}}}\right\} + \left[\mathbf{C_1}\right]\left\{\dot{\hat{\mathbf{z}}}\right\} + \left[\mathbf{K_1}\right]\left\{\hat{\mathbf{z}}\right\} = \left\{\hat{\mathbf{F}}_{eq}\right\}. \tag{3.10}$$

where, $[\mathbf{M_1}]$, $[\mathbf{C_1}]$ and $[\mathbf{K_1}]$ are (6×6) inertia, damping and stiffness matrices, respectively, $\left\{\hat{\mathbf{F}}_{eq}\right\}$ is (6×1) force vector and $\{\hat{\mathbf{z}}\}$ is (6×1) generalized displacement coordinate vector. These matrices are further defined in Appendix A.

3.2 Experimental Validation of HAS Model

To ensure that the response of the HAS model with and without a glove (described in the 'Mathematical Formulation' section) matches with the response of a real human HAS, we compare the HAS model's response at the palm and finger against the experimental results measured at the palm and finger of a human being. To perform this comparison, we use unweighted relative transmissibility and is defined below.

$$(t_p)_{without\ glove} = \frac{z_p}{Z_0}\,,$$
$$(t_f)_{without\ glove} = \frac{z_f}{Z_0}\,. \tag{3.11}$$

Similarly, the unweighted transmissibilities of the palm and fingers with a glove are defined as

$$(t_p)_{with\ glove} = \frac{(z_p)_{with\ glove}}{Z_0}\,,$$
$$(t_f)_{with\ glove} = \frac{(z_f)_{with\ glove}}{Z_0}\,. \tag{3.12}$$

Then the 'relative transmissibilities' at the palm and fingers [20] are defined as

$$T_p = \frac{(t_p)_{with\ glove}}{(t_p)_{without\ glove}}\,,$$
$$T_f = \frac{(t_f)_{with\ glove}}{(t_f)_{without\ glove}}\,. \tag{3.13}$$

The parameters used for this part of the exercise correspond to a gel-filled glove, as reported by Dong *et al.* [20]. To obtain the model's relative transmissibility response, the numerical time response of the system to broadband random excitation, with a flat power spectral density of $3.0(m/s^2)^2/Hz$, is obtained using MATLAB routine 'ode45'. Afterward, the system's frequency response is obtained using the fast fourier transform on the time response, obtained using the MATLAB built-in command 'fft'. Further, the experimental transmissibility data at the palm is obtained using the palm adapter method [16]. While, the experimental transmissibility data at the finger is obtained using the experimental biodynamic method [20].

The comparison between the experimental and model response data against each other is shown in Fig. 3.2. From Fig. 3.2, the experimental data and model responses match with a few discrepancies as also noted in [20]. For the finger response, the modeled transmissibility values deviate from the experimental transmissibility values at frequencies less than 100Hz. Apart from these deviations, the response of the model is fairly consistent with the response obtained experimentally. As such, we proceed using the model responses to analyze the AV glove.

The analytical solutions of these coupled second order ODEs for the hand-arm system with and without gloves (Eqs. (3.10) and (3.5)) are presented in the next section.

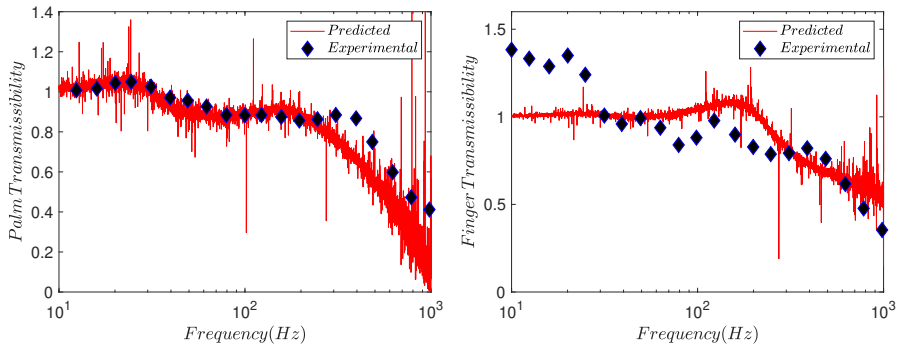

(a) (b)

Figure 3.2: Comparison of the HAS model relative transmissibility response with experimental transmissibility response at the a) Palm and at the b)Finger.

3.3 Analytical solution for HAS

In this section, we briefly present the method of harmonic balance (i.e.,undetermined coefficient method) to solve the equations of motion governing the dynamics of the hand-arm system with and without gloves. For the current analysis, we employ a harmonic excitation in the form of

$$z(t) = Z_0 \cos(\omega t) \ , \tag{3.14}$$

where Z_0 and ω are the amplitude and frequency of the external excitation, respectively. At this stage, we look for the solutions synchronous with external excitation and hence, without any loss of generality we assume the solutions of Eqs. (3.5) and (3.10) in the form of

$$\{\mathbf{z}\}(t) = \{\mathbf{A}\}\cos(\omega t) + \{\mathbf{B}\}\sin(\omega t)\ , \tag{3.15}$$

$$\{\hat{\mathbf{z}}\}(t) = \{\mathbf{A_1}\}\cos(\omega t) + \{\mathbf{B_1}\}\sin(\omega t)\ , \tag{3.16}$$

where $\{\mathbf{A}\}$ and $\{\mathbf{B}\}$ are (4×1) columns vectors with unknown coefficients $A_i's$ and $B_i's$ $(i = 1 \cdots 4)$the , respectively, and, $\{\mathbf{A_1}\}$ and $\{\mathbf{B_1}\}$ are (6×1) columns vectors with unknown coefficients $A_{1i}'s$ and $B_{1i}'s$ $(i = 1 \cdots 6)$, respectively. On substituting $\{\mathbf{z}\}$(t) and $\{\hat{\mathbf{z}}\}(t)$ in Eqs (3.5) and (3.10), respectively, we get

$$\begin{aligned}
&-\omega^2[\mathbf{M}]\{\mathbf{A}\}\cos(\omega t) - \omega^2[\mathbf{M}]\{\mathbf{B}\}\sin(\omega t)\\
&-\omega[\mathbf{C}]\{\mathbf{A}\}\sin(\omega t) + \omega[\mathbf{C}]\{\mathbf{B}\}\cos(\omega t) + [\mathbf{K}]\{\mathbf{A}\}\cos(\omega t)\\
&+[\mathbf{K}]\{\mathbf{B}\}\sin(\omega t) = \{\mathbf{F_{eq}}\}\ ,
\end{aligned} \tag{3.17}$$

$$\begin{aligned}
&-\omega^2[\mathbf{M}_1]\{\mathbf{A_1}\}\cos(\omega t) - \omega^2[\mathbf{M}_1]\{\mathbf{B_1}\}\sin(\omega t)\\
&-\omega[\mathbf{C}_1]\{\mathbf{A_1}\}\sin(\omega t) + \omega[\mathbf{C}_1]\{\mathbf{B_1}\}\cos(\omega t)\\
&+[\mathbf{K}_1]\{\mathbf{A_1}\}\cos(\omega t) + [\mathbf{K}_1]\{\mathbf{B_1}\}\sin(\omega t) = \left\{\hat{\mathbf{F}}_{eq}\right\}.
\end{aligned} \tag{3.18}$$

By equating the coefficients of sine and cosine on both sides of Eqs. (3.17) and (3.18) we obtain two sets of algebraic equations corresponding to the ungloved and gloved hand, respectively. On solving these linear algebraic equations we get $\{\mathbf{A}\}$, $\{\mathbf{B}\}$, $\{\mathbf{A1}\}$ and $\{\mathbf{B1}\}$, and accordingly, the amplitude vectors $\{\mathbf{z}\}$ and $\{\hat{\mathbf{z}}\}$ (Eqs. (3.15) and (3.16)). The closed form expressions of the elements of these amplitude vectors are very complex and hence, for

the sake of brevity are not reported. A detailed analysis of the systems, i.e., HAV with and without gloves, using the analytical solutions is presented in the next section.

Chapter 4

Results and discussion

In this section, the analytical solution of the system, obtained in Chapter 3, is verified using numerical solutions. Thereafter, a parametric study is performed to analyze the effectiveness of the anti-vibration gloves against the transmitted vibrations. The mechanical properties of the hand-arm system and glove, used for the numerical simulations, are presented in Table 4.1. For the sake of simplicity in the parametric analysis, the numerical values of m_{g2}, m_{g4}, m_{g6}, k_7, c_7 are kept proportional to m_{g1}, m_{g3}, m_{g5}, k_6, c_6, respectively.

4.1 Verfication of Analytical Solution for HAS Model

The first part of the analysis is to validate the obtained analytical solutions by comparing them against the numerical simulations of Eqs. (3.5) and (3.10). The comparison between numerical solutions from Eqs. (3.5), (3.10) and analytical solutions from Eqs. (3.15) and (3.16) are presented for $m_{g2} = m_{g1}$, $m_{g4} = m_{g3}$, $m_{g6} = m_{g5}$, $k_7 = k_6$ and $c_7 = c_6$. The initial conditions for numerical simulations are chosen corresponding to steady state response. For the numerical simulations of Eqs. (3.5) and (3.10), we have used the built-in command 'ode45' in Matlab with very tight absolute tolerance and relative tolerance ($1e^{-10}$).

To compare the analytical solutions and numerical simulations, we have used the responses of palm and finger (z_p and z_f), and are shown in Fig. 4.1. Figures 4.1(a) and 4.1(b) represent the responses of the fingers and palm without gloves respectively, while Figures 4.1(c) and 4.1(d)

Table 4.1: Parameters of the hand-arm system and glove based on parameters of a gel-filled glove determined in [20].

Parameter	Value	Units	Parameter	Value	Units	Parameter	Value	Units
m_0	6.015	(kg)	k_0	7567	N/m	c_0	106	Ns/m
m_p	1.4618	(kg)	k_w	2978	N/m	c_w	134	Ns/m
m_f	0.0958	(kg)	k_1	4221	N/m	c_1	52	Ns/m
m_{tp}	0.0338	(kg)	k_2	196038	N/m	c_2	122	Ns/m
m_{tf}	0.0186	(kg)	k_3	55564	N/m	c_3	126	Ns/m
m_{g1}	0.0674	(kg)	k_4	2417	N/m	c_4	1	Ns/m
m_{g3}	0.0651	(kg)	k_5	0	N/m	c_5	0	Ns/m
m_{g5}	0.0005	(kg)	k_6	454779	N/m	c_6	106	Ns/m
m_H	3	(kg)	k_s	940	N/m	c_s	79	Ns/m

represent the responses of the fingers and palm with gloves, respectively. From Fig. 4.1, we can observe that there is an excellent agreement between the numerical simulations and analytical solutions for the given values of system parameters. This agreement further improves with the increase in time steps. Therefore, in the remainder of this work, we use the analytical solutions for the analysis. Having obtained the solution for the response of different parts of the hand-arm system, the effect of different glove parameters on the unweighted glove transmissibility (as defined in Eqs. (3.11) and (3.12) are shown.

4.2 Parametric study of AV gloves

The comparison of palm's transmissibility with and without an AV glove for different glove parameters has been shown in Fig. 4.2. In this figure, the peak value of the curve represents the instance of primary resonance. However, the frequency corresponding to the second and third resonance is not evident. From Fig. 4.2, it also seems that the transmissibility response of the palm with the glove is almost similar to the one without the glove and is independent of the glove's parameters.

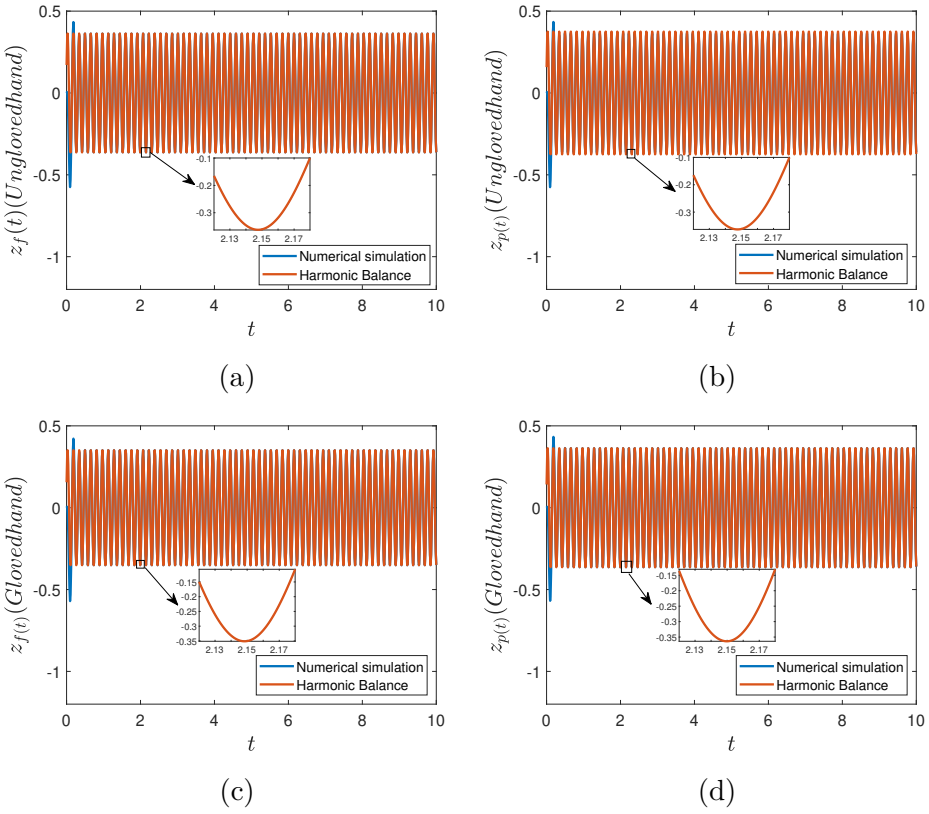

Figure 4.1: Comparison of numerical and analytical solutions for the responses of (a) fingers without gloves, (b) palm without gloves, (c) fingers with gloves, and (d) palm with gloves. The other parameters are chosen as $Z_0 = 1$, $\omega = 40\frac{rad}{s}$, $m_{g2} = m_{g1}$, $m_{g4} = m_{g3}$, $m_{g6} = m_{g5}$, $k_7 = k_6$ and $c_7 = c_6$

To make these figures easier to read, the transmissibility data, with different masses of the AV gloves, is displayed on a log-log scale. As shown in Fig. 4.3(a), the first resonance peak is evident while the appearance of the second resonance peak is slightly apparent. However, similar to the data presented on a linear scale (Fig. 4.2), it is difficult to observe the impact of different masses of the glove on the transmissibility at the palm on the log scale. To make sure this phenomenon was not unique to the palm, the parametric study analyzing the effects of the glove's mass was also performed while examining transmissibility at the fingers. As seen from Fig. 4.3(b), it is almost impossible to distinguish between the transmissibility plots for different masses of the AV glove, even though the appearance of resonance peaks on the transmissibility plot is more apparent. Therefore, to have a better understanding of

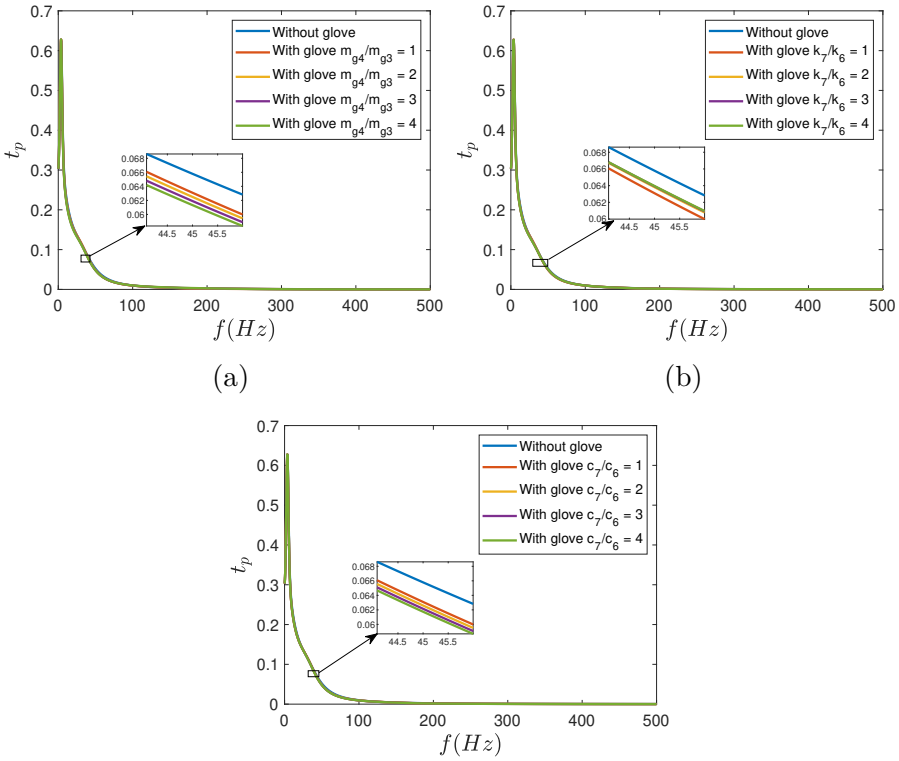

Figure 4.2: Comparison of palm transmissibility curves with and without gloves with different glove parameters.

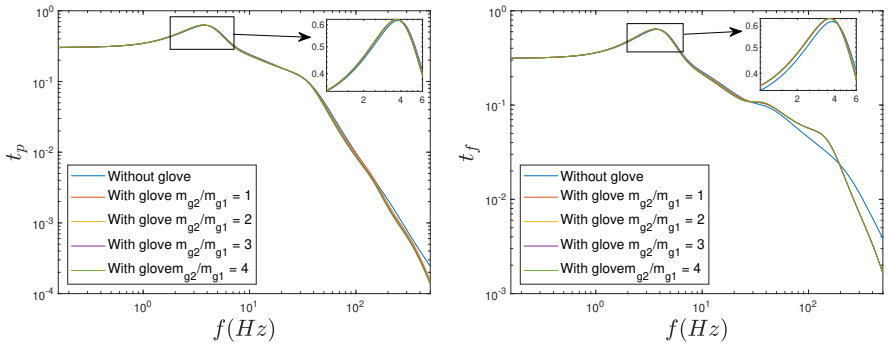

Figure 4.3: Comparison of palm and finger transmissibility curves with and without gloves with different glove parameters on axes with logarithm scales.

the effectiveness of the AV glove and role of different glove parameters, we use the relative transmissibility(as defined in Eqs. (3.13)).

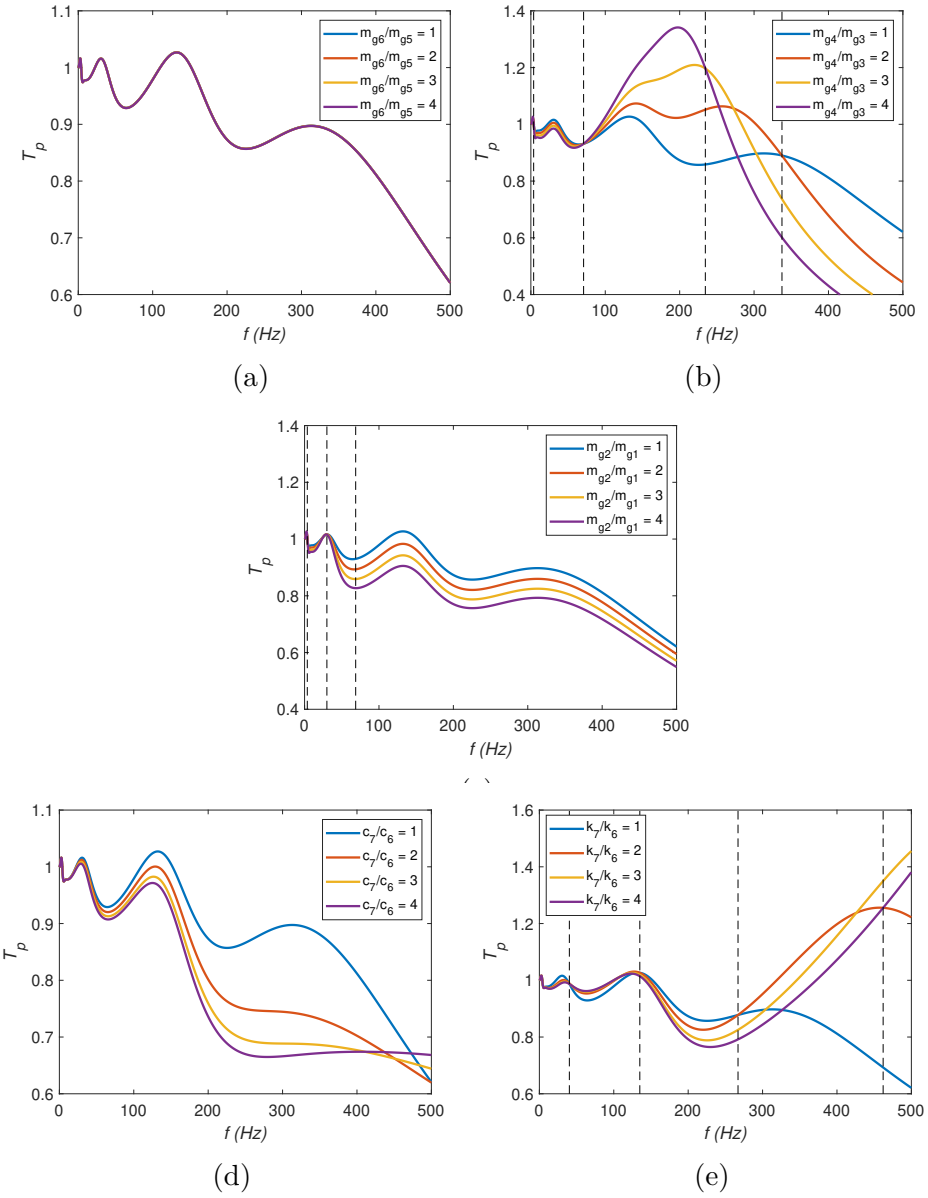

Figure 4.4: Comparison of relative palm transmissibility curves with different glove parameters.

The effect of different glove parameters on the relative transmissibilities is depicted in Fig. 4.4 and Fig. 4.5. From these figures, we observe that the instances of the primary and secondary resonances are more evident in relative transmissibility than in absolute transmissibility. Also, the effect of the glove parameters on the glove's performance is clearly visible through relative transmissibility.

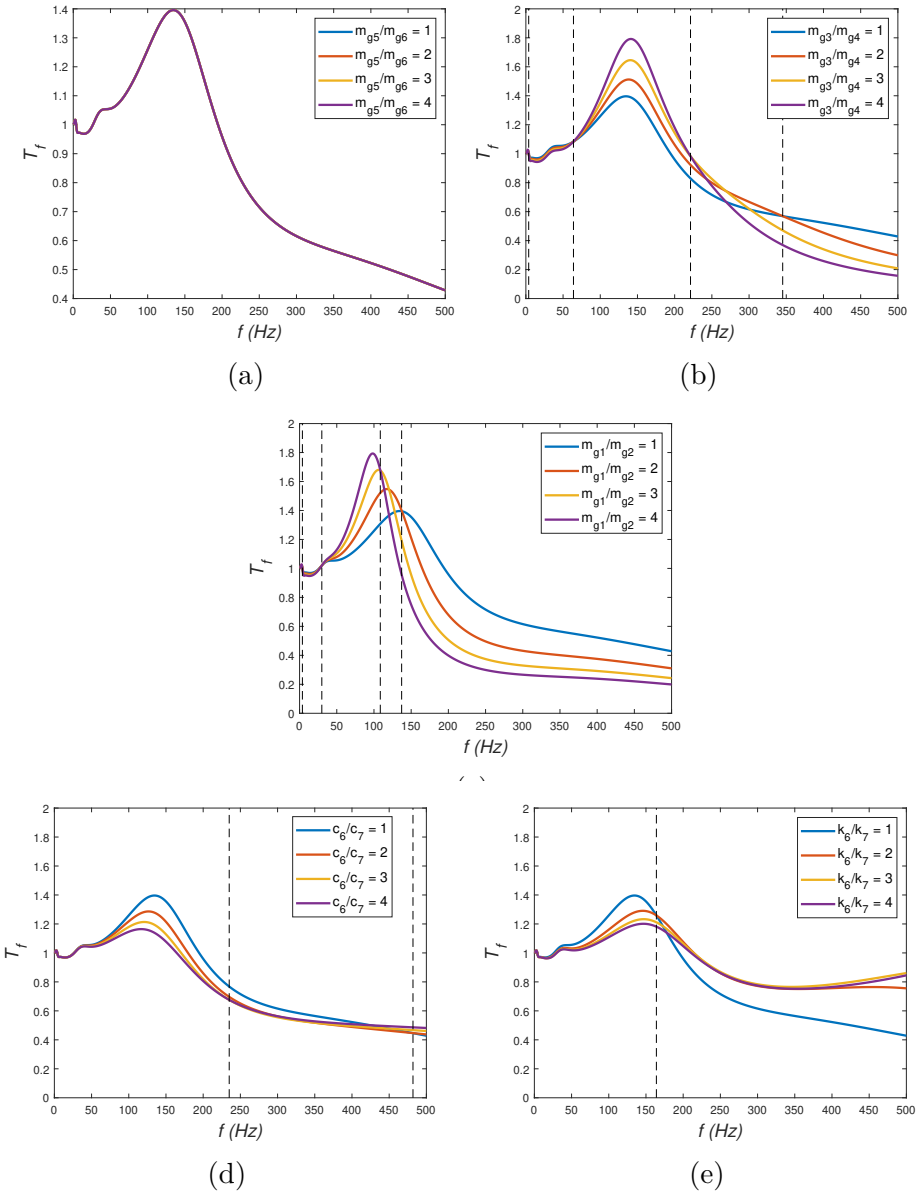

Figure 4.5: Comparison of relative finger transmissibility curves with different glove parameters.

For instance, the masses of the glove in direct contact with the handle does not influence the transmissibility significantly. However, the other glove parameters, which are in direct contact with the hand, significantly influence the performance of the glove.

Changing properties of the glove materials in direct contact with the palm results in relative transmissibility at the palm with significant differences, i.e., changing m_{g4}, m_{g2}, c_7 and k_7.

From Fig. 4.4b increasing m_{g4}, results in a decrease in transmissibility between 3Hz and 70 Hz and 337Hz to 500Hz. Between 70Hz and 234 Hz, an increase in m_{g4} causes an increase in transmissibility, and from 234Hz to 337 Hz, there is no specific trend in how transmissibility changes with an increase in m_{g4}.

When m_{g2}, is increased the transmissibility decreases between 3Hz and 500Hz as shown in Fig. 4.4c. It is worth noting that at 30Hz the transmissibility values for the different values of m_{g2} converge at the same value.

An increase in the damping parameter of the glove at the palm side, c_7, causes transmissibility at the palm to decrease(Fig. 4.4d). It can be seen that as the frequency increases, the difference in transmissibility for the different values of c_7 increase.

Between 5Hz to 40Hz and 135Hz to 267Hz, an increase in the stiffness of the glove k_7 causes a decrease in transmissibility. From 40Hz to 135Hz and 462Hz to 500Hz, an increase in k_7 causes transmissibility to increase. Between 267Hz to 462Hz we observe no specific trend in how transmissibility changes with an increase in k_7.

As with the palm, changing properties of the glove materials in direct contact with the finger results in different transmissibility curves with significant differences, i.e., changing m_{g3}, m_{g1}, c_6 and k_6.

As seen in Fig. 4.5b, an increase in m_{g3} causes the transmissibility between 3.8Hz to 63.98Hz and 345.2Hz to 500Hz at the finger to decrease. From 63Hz to 221Hz the transmissibility at the finger increases when m_{g3} is increased. Between 221Hz and 345Hz, there is no distinctive trend in how transmissibility changes with changing m_{g3}.

When m_{g1} is increased, the dominant resonant peaks, apparent in the transmissibility curve shifts to a higher frequency ,i.e, Fig. 4.5c. Also, between 3Hz to 29Hz and 137Hz to 500Hz, increasing m_{g3} decreases transmissibility. While between 29Hz and 108Hz, an increase in

m_{g1} leads to an increase in transmissibility.

Fig. 4.5d shows the change in transmissibility with different values of c_6. Between 0Hz and 235Hz, an increase in c_6 causes transmissibility at the finger to decrease and between 482Hz and 500Hz an increase in c_6 leads to an increase in transmissibility. Between 235Hz and 482Hz, there is no distinctive trend in how the transmissibility changes with an increase in c_6.

Finally, when k_6 is increased a decrease in transmissibility is observed between 0Hz and 164Hz as shown in Fig. 4.5e. Between 164Hz and 500Hz, there is no distinctive trend in how the transmissibility changes with an increase in k_6.

From Fig. 4.4 and Fig. 4.5 , we can observe that the effect of different glove parameters on the relative transmissibility is not uniform over a wide frequency range, in our case 0-500 Hz. Therefore, it is not possible to select global key parameters of the glove, which can enhance the performance of AV glove over a wide frequency range. Instead depending on the excitation frequency, key design parameters of glove can decided to enhance the performance. In other to provide a more in-depth study of the effect of the glove parameters on transmissibility, the effect of damping is more closely studied.

It is a well-established fact that damping in some dynamical systems plays a vital role in achieving better transmissibility [47]. Therefore, it is necessary to better understand the effects of damping properties of different parts of gloves on its performance. To assess the effect of damping on the performance of an AV glove, we compare relative finger and palm transmissibilities corresponding to the excitation frequencies in the amplification (f_A) and isolation zones (f_I) with varying values of damping parameters of the AV glove. Excitation frequencies in the isolation region of either the palm or finger satisfy the relation:

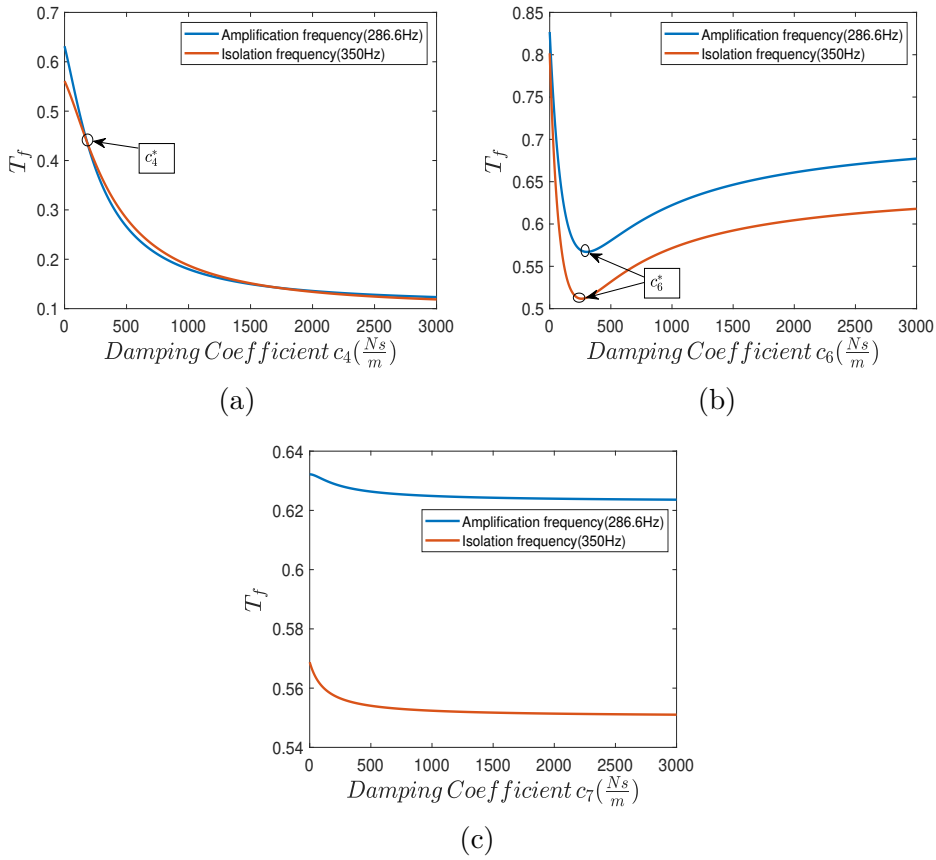

Figure 4.6: Comparison of the relative finger transmissibility curves for the frequencies in amplification (f_A = 286.6 Hz) and isolation zone (f_I = 350 Hz) with different damping values of glove (a) connecting finger and palm (c_4), (b) connecting handle and finger-tip (c_6), and (c) connecting handle and palm-tip (c_7).

$$\frac{\omega_{excitation}}{\omega_{naturalfrequency,finger/palm}} > \sqrt{2}\,,$$

while excitation frequencies in the amplification region of either the palm or finger satisfy the relation:

$$\frac{\omega_{excitation}}{\omega_{naturalfrequency,finger/palm}} < \sqrt{2}\,,$$

The amplification region of the fingers and palm corresponds to the excitation frequencies below $322Hz$ and $43Hz$, respectively. Similarly, the isolation region of the fingers and palm

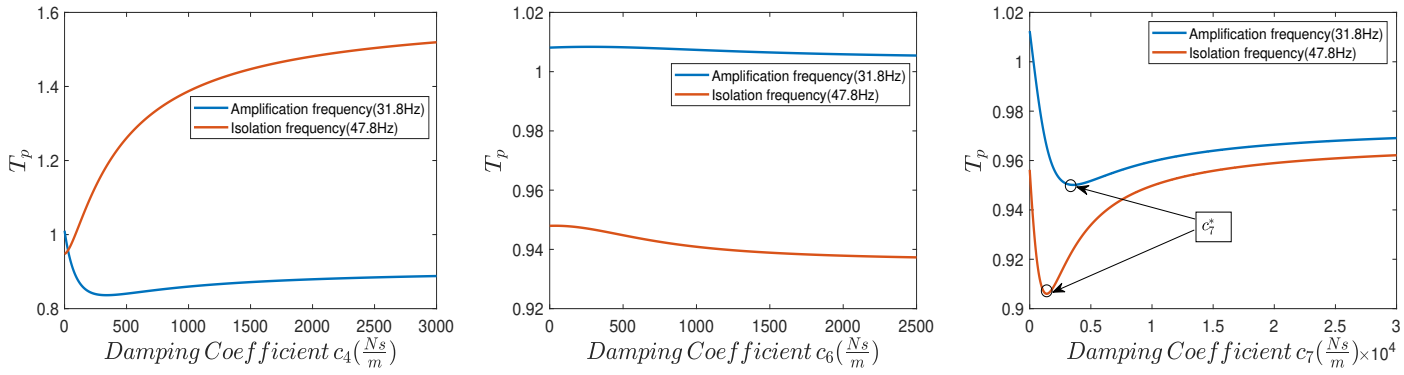

(a) (b) (c)

Figure 4.7: Comparison of the relative palm transmissibility curves for the frequencies in amplification ($f_A = 31.8$ Hz) and isolation zone ($f_I = 47.8$ Hz) with different damping values of glove (a) connecting finger and palm (c_4), (b) connecting handle and finger-tip (c_6), and (c) connecting handle and palm-tip (c_7)

corresponds to the excitation frequencies above $322Hz$ and $43Hz$, respectively.

Figure 4.6 depicts the variation of the relative finger transmissibilities, for f_A and f_I, with different damping properties of the glove. From Figure. 4.6a, we can observe that with an increase in c_4, the relative transmissibility decreases irrespective of the excitation frequencies. However, this observation does not hold any longer for the case of c_6 and c_7. From Fig. 4.6b, we observe that the relative transmissibility first decreases with an increase in the value of c_6 and reaches a minimum value at c_6^*. With a further increase in c_6 after c_6^*, the relative transmissibility starts increasing again and asymptotically reaches a constant value. A similar observation can be drawn for the case of c_7 also, i.e., with an increase in c_7, the relative transmissibility decreases and asymptotically reaches a constant value.

Further, we observe that the relative finger transmissibility corresponding to f_I always remains lower than the transmissibility corresponding to f_A irrespective of the value of c_6 and c_7. This further implies that the choices of c_6 and c_7 for better isolation are independent of amplification and isolation zones. However, this observation does not hold any longer for the

case of c_4. As the value of c_4 increases, the relative finger transmissibility corresponding to f_A becomes lower than the transmissibility corresponding to f_I after a critical value of $c_4(c_4^*)$. However, with a further increase in c_4,the relative finger transmissibility corresponding to f_A again becomes more significant than the transmissibility corresponding to f_I. These observations further help in deciding the ranges of damping parameters to get better vibration isolation for the fingers.

Now, we look for the effects of different damping parameters on the relative palm transmissibility. From Figure. 4.7a, we observe that only low values of c_4 provide better isolation at the palm for the excitation frequency corresponding to the amplification zone. However, this observation is not valid for the case of excitation frequency in the isolation zone. Figure. 4.7c shows that with an increase in c_7 the transmissibility of the palm decreases to a minimum value at c_7^* after which it increases again and asymptotically reaches a constant value. Further, we observe that c_6 has no significant effect on the performance of AV glove for the vibration isolation of palm (Fig. 4.7b).

These observations further help to guide the way various parameters in an anti-vibration glove are tuned; thus ensuring maximum vibration attenuation at a specific frequency, at which they may be employed. Also, we observe the effect of the parameters studied on the performance of glove is not monotonous and changes from one frequency to another frequency. This observation is consistent with earlier findings that the performance/effectiveness of the AV glove significantly depends on the application and, consequently, on the frequency of the external excitation.

With this motivation, we optimize the glove parameters to minimize the overall transmissibility and this is presented in the next section.

Chapter 5

Optimization

5.1 Single-objective Optimization

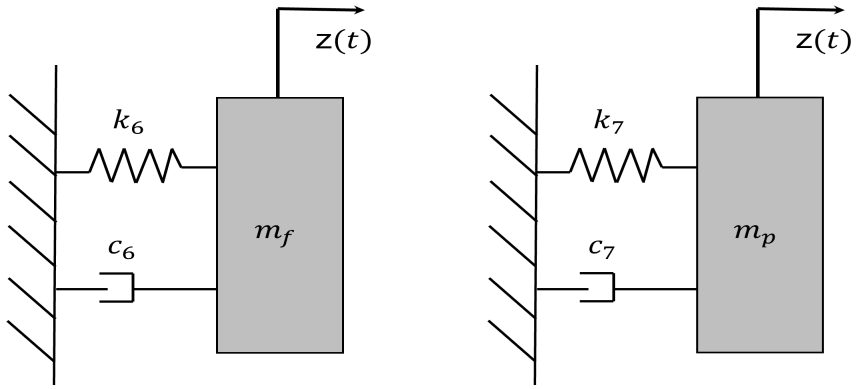

(a) (b)

Figure 5.1: Main mass of (a) finger and (b)palm on estimated equivalent suspension .

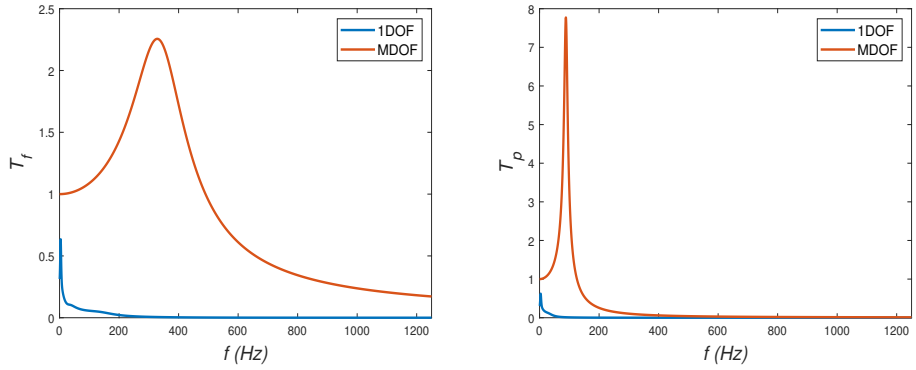

(a) (b)

Figure 5.2: Comparison of relative (a) finger transmissibility and (b) palm transmissibility curves for approximation of Gloved hand-arm system as one degree of freedom system.

As a first step towards optimizing the parameters of the AV glove, we assume that the motion

of the palm and finger, described by the MDOF, can be estimated by a 1DOF mass-spring damper system. We consider the main masses of the finger and palm to be on the equivalent visco-elastic suspensions k_6 and c_6, and c_7 and k_7 respectively as shown in Fig. 5.1a and b.

This assumption is made so that the optimized 1DOF model values for the stiffness and damping parameters(k_6, c_6, c_7 and k_7) can give a fair estimate on what the visco-elastic optimal parameters would be when the MDOF system is optimized.

When two springs are connected in series, the larger stiffness of the two springs has a greater effect on the resulting effective stiffness of both springs in comparison to the smaller spring. As such, the visco-elastic properties k6 and c6 are chosen as the equivalent suspension for the finger. Since k6 is the greater of the two suspensions, between the palm and the steeringhandle, when k6 and k2 are compared. Also, the visco-elastic properties k_7 and c_7 are chosen as the equivalent suspension for the palm. Since k_7 is the greater of the two suspensions, between the palm and the steering handle when k_7 and k_8 are compared. The values of this parameters are listed in Table 4.1.

In order to optimize the glove parameters, we start of by verifying the validity of the estimated model. The transmissibility curves for the 1DOF and MDOF when both systems are exposed to a harmonic excitation z(t), as defined in Eq. 3.14, is obtained. From Fig. 5.2b, it can be seen that the 1DOF model estimates the transmissibility at the palm fairly between 400Hz and 1250Hz. However, the 1DOF model estimate for the finger does not estimate the transmissibility at the palm correctly. As such, the parameters for just the palm's 1DOF model are studied.

To obtain the visco-elastic properties which best reduce transmissibility, the transmissibility of the 1DOF system for the palm is obtained for different values of k_7 and c_7. From Fig. 5.3a and b, we obtain the smallest transmissibility when the visco-elastic properties are smallest.

This result implies that the glove parameters, c_7 and k_7, which best optimize transmissibility at the palm in the high frequency range will have visco-elastic properties that are relatively small given some optimization bounds.

However, this optimization result does not reveal the values to which the other visco-elastic properties of the glove should be set to in order to optimize the glove transmissibility at the finger and the palm. As such we present multi-objective optimization.

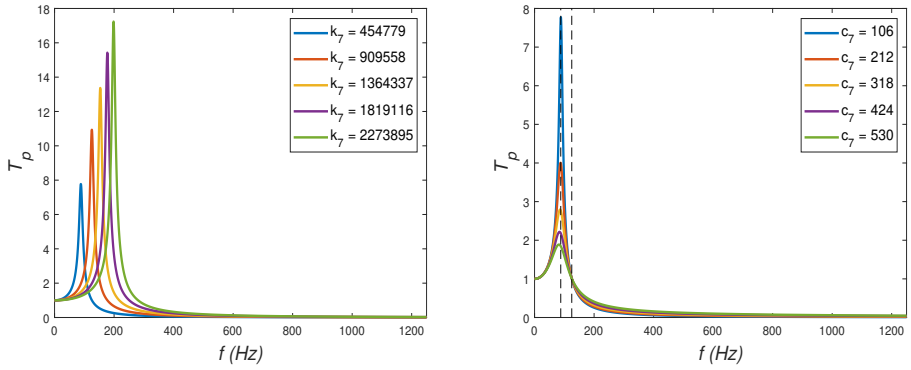

(a) (b)

Figure 5.3: Transmissibility of 1DOF system for varying values of a)k_7 and b)c_7.

5.2 Multi-objective Optimization

In this section, we present the optimization of the AV glove parameters for better isolation performance. Since the palm and fingers are in direct contact with the vibrating steering wheel, we optimize the glove parameters to minimize both, i.e., palm and finger relative transmissibility together. To perform the multi-objective optimization, we have used Matlab's built-in function 'gamultiobj'. These optimization simulations have been performed with relatively larger number of initial points, more specifically 10^5, to ensure the convergence of glove parameters towards optimum values. 'gamultiobj' returns the value of optimized parameters on the Pareto front of objective functions (set of inferior objective

function values in the space of objective functions).

Note that it is more beneficial to design a glove with optimal parameters for a specific application rather than for a global purpose. On considering this fact, we perform multi-objective optimization for three different frequency ranges. More specifically anti-vibration gloves are optimized for a low frequency (5Hz to 25Hz), medium frequency (25Hz to 200Hz) and high frequency (200Hz to1250Hz) range.

Further, for the sake of simplicity in the analysis, we consider that the properties of the steering wheel do not change in these different frequency ranges. Therefore, we are designing the anti-vibration glove for different vehicles with varying excitation frequencies due to factors such as road terrain or vehicle type. Even though the optimization results presented in this section are particular to the system with the steering wheel described, the optimization technique employed is meant to apply to a wide variety of tools whose mass and visco-elastic properties are different from the vibrating equipment described in this paper.

Before proceeding further, we define weighted palm and finger's transmissibility for optimization. According to the ISO standard 10819 [48], the weighted transmissibilities at the palm and fingers, without a glove (wng) are defined as:

$$
\begin{aligned}
(t_p)_{wng} &= \frac{\sqrt{\sum_{i=i_L}^{i_u} \left[(z_p)_{without\,glove} * \omega_i^2 * W_{hi} \right]^2}}{\sqrt{\sum_{i=i_L}^{i_u} \left[Z_0 * \omega_i^2 * W_{hi} \right]^2}}, \\
(t_f)_{wng} &= \frac{\sqrt{\sum_{i=i_L}^{i_u} \left[(z_f)_{without\,glove} * \omega_i^2 * W_{hi} \right]^2}}{\sqrt{\sum_{i=i_L}^{i_u} \left[Z_0 * \omega_i^2 * W_{hi} \right]^2}}.
\end{aligned}
\tag{5.1}
$$

Similarly, the weighted transmissibilities at the palm and fingers with the glove (wg) can be

written as:

$$(t_p)_{wg} = \frac{\sqrt{\sum_{i=i_L}^{i_u} \left[(z_p)_{with\,glove} * \omega_i^2 * W_{hi}\right]^2}}{\sqrt{\sum_{i=i_L}^{i_u} \left[Z_0 * \omega_i^2 * W_{hi}\right]^2}},$$
$$(t_f)_{wg} = \frac{\sqrt{\sum_{i=i_L}^{i_u} \left[(z_f)_{with\,glove} * \omega_i^2 * W_{hi}\right]^2}}{\sqrt{\sum_{i=i_L}^{i_u} \left[Z_0 * \omega_i^2 * W_{hi}\right]^2}}. \tag{5.2}$$

In these expressions, both i_L and i_u represent one-third-octave frequency band numbers, ω_i is the one-third-octave center frequency for the i^{th} one-third-octave band, and W_{hi} represents the frequency weighting corresponding to each i^{th} band number as shown in ISO 10819. Fig. 5.8 shows the frequency weighting for the hand-arm system at various frequencies. For the low frequency range, i_L is set to 6 and i_u is set to 14. For the medium frequency range, i_L is set to 14 and i_u is set to 23. For the high frequency range, i_L is set to 23 and i_u is set to 31. The values for the frequency weighting for the low frequency range are obtained from [49]. Therefore, the relative weighted transmissibility for the palm and finger i.e., T_{pw} and T_{pf}, respectively, are defined as

$$T_{pw} = \frac{(t_p)_{wg}}{(t_p)_{wng}}, \tag{5.3}$$

$$T_{fw} = \frac{(t_f)_{wg}}{(t_f)_{wng}}. \tag{5.4}$$

In a next step, we define our objective or fitness function for the 'gamultobj' as

$$objective\ function = min(T_{pw}, T_{fw}),$$
$$\{\mathbf{lb}\} \leq \{\mathbf{x}\} \leq \{\mathbf{ub}\},$$

where $\{\mathbf{x}\}$ represents the vector containing glove parameters to be optimized, and is given

by

$$\{\mathbf{x}\} = \{m_{g3}\,, k_4\,, k_5\,, k_6\,, k_7\,, c_4\,, c_5\,, c_6\,, c_7\}.$$

Also, $\{\mathbf{lb}\}$, and $\{\mathbf{ub}\}$ represent the lower and upper bounds of the parameters respectively, and are given by

$$\{\mathbf{lb}\} = \{0.0001,\ 10^3,\ 10^3,\ 10^5,\ 10^5,\ 0.0001,\ 0.0001,\ 10,\ 10\}$$

and

$$\{\mathbf{ub}\} = \{0.1302,\ 2417,\ 2417,\ 10^6,\ 10^6,\ 1,\ 1,\ 200,\ 200\}.$$

These parameters have the same units as the parameters of the glove defined in Table 4.1. The other parameters of the optimization glove are not changed to avoid adding weight to the anti-vibration glove. Since anti-vibration gloves are supposed to be more effective at the fingers, we decided to optimize the glove mass in direct contact with fingers, i.e., m_{g3} (Fig. 3.1). The upper bounds for m_{g3} of the glove are obtained by doubling the value of m_{g3} shown in Table 4.1. The lower bound for the gloves mass parameter is assumed to be the smallest glove mass (m_{g5}) rounded down to the nearest power of 10.

The upper bounds for the elastic properties of the glove k_6 and k_7 are determined by rounding up their values presented earlier to the nearest power of 10. However, the upper bounds for the viscous properties of the glove c_6 and c_7 are determined by rounding up their value to the nearest multiple of 100. The lower bounds for k_6, k_7, c_6 and c_7 are then determined by rounding down their values from Table 4.1 to the nearest power of 10.

Furthermore, Wimer *et al.* [83] observed that the high stiffness of anti-vibration gloves elements, connecting the elements of gloves in direct contact with finger and palm (k_4), causes

a reduction in the grip strength as compared to grip strength without gloves. This reduction in the grip strength can be compensated for by exerting more pressure from the human hand. However, high grip strength values while operating machinery can be detrimental to the operators of the machinery. Therefore, it is required that anti-vibration gloves are design such that minimal grip strength is exerted while operating a machinery. With the consideration of this observation, the upper bound of glove parameters responsible for grip strength, i.e., k_4, k_5, c_4, c_5 were chosen to the respective maximum values of glove parameters studies in earlier section. More specifically, the upper bounds of k_4 and k_5 are chosen as 2417, whereas, the upper bounds of c_4 and c_5 are chosen as 1. The lower bounds of the glove properties, k_4 and k_5, were chosen to be the presented values of k_4 nd k_5 rounded down to the nearest power of 10. While the lower bounds for c_4 and c_5 were chosen to be 10^{-4}.

We use these upper and lower bounds of the variables as the input arguments for 'gamultiobj' to get the optimized values of variables of interest. Note that as we are performing multi-objective optimization, we get a number of optimized solutions instead of a unique solution. The objective function values corresponding to these optimal solutions are shown in Fig. 5.4 on a Pareto front for three different frequency ranges. From Fig. 5.4, we can observe that there is always a trade-off between two objective functions, i.e., a true minima point of T_{pw} does not coincide with the true minima of T_{fw}. To elaborate this observation further, we show three different set of optimal solutions for low, middle and higher frequency ranges in Tables 5.1, 5.2 and 5.3, respectively. We emphasize that although all three sets are feasible solutions to our optimization problem, Set 1 and Set 3 correspond to min T_{pw} and min T_{fw}, respectively, while Set 2 provides trade-off values of T_{fw} and T_{pw}. To avoid any preference of one objective element over another element, we have used Set 2 as our optimized solution candidate for further analysis.

From Tables 5.3 we observe that the c_7 and k_7 which minimize palm transmissibility in the

Table 5.1: Comparison of optimal parameters obtained from Pareto front for low frequency range.

	m_{g3}	k_4	k_5	k_6	k_7	c_4	c_5	c_6	c_7	T_{pw}	T_{fw}
Set 1	0.1302	1239.34	1771.85	10^6	10^6	1	1	62.67	200	0.9629	0.9547
Set 2	0.1302	2417	1770.89	10^6	10^6	1	1	62.63	200	0.9630	0.9514
Set 3	0.1302	2417	1762.32	10^6	10^6	0	0.0304	135.6	105.92	0.9639	0.9507

Table 5.2: Comparison of optimal parameters obtained from Pareto front for medium frequency range.

	m_{g3}	k_4	k_5	k_6	k_7	c_4	c_5	c_6	c_7	T_{pw}	T_{fw}
Set 1	0.1302	1053.87	1312.4	$9.75(10^5)$	10^5	1	1	200	200	0.8404	1.1263
Set 2	0.1302	1054.14	1320.45	10^5	10^5	1	1	200	200	0.8617	0.9449
Set 3	0.000105	2327.66	1202.8	10^5	$9.65(10^5)$	1	1	200	198.9721	1.0008	0.9067

Table 5.3: Comparison of optimal parameters obtained from Pareto front for high frequency range.

	m_{g3}	k_4	k_5	k_6	k_7	c_4	c_5	c_6	c_7	T_{pw}	T_{fw}
Set 1	0.1302	1166.98	1424.9	10^5	10^5	1	1	10	53.78	0.3058	0.2164
Set 2	0.1302	10^3	10^3	10^5	10^5	1	0	16.6	50.58	0.3135	0.2145
Set 3	0.1302	10^3	10^3	10^5	10^5	1	0	17.6544	10.0004	0.3605	0.2142

high frequency range settle close to the lower bounds set to the multi-objective optimization scheme as indicated in Section 5.1.

Furthermore, from Tables 5.1 and 5.3, we can observe that optimum values of k_6 and k_7 settle down to their high and lower bounds for the low and high frequency ranges respectively. This observation can be justified from the aspect of vibration isolation of a single-degree of freedom system. In an isolation zone (higher frequency range in our case), lower stiffness of an isolator leads to better isolation. However, for very low excitation frequencies, high stiffness of the isolator provides better performance. Having established the solution candidate for the optimized glove, we present the comparison of the performance of optimized glove against the gel-filled glove. For this, we compare the relative transmissiblity for the optimized glove and gel-filled glove in the low, medium and high-frequency ranges and are shown in Figs.

5.5, 5.6 and 5.7, respectively.

From Fig. 5.5 we can observe that the anti-vibration glove, with optimum glove parameters, is more effective at attenuating vibrations in the low frequency region at the fingers than the anti-vibration glove described in Table 4.1. The optimized anti-vibration glove isolates rather than amplifies vibration to the finger unlike most typical anti-vibration gloves [22].

In both the medium and high frequency ranges as seen in Fig. 5.6, the optimal AV glove performs better than the glove described in Table 4.1. Therefore an anti-vibration glove designed with these parameters may help attenuate high frequency vibrations from tools such as etching pens, rotary files and chainsaws.

Even though the optimized AV glove parameters presented above may not be physically realizable, the multi-objective study reveals what parameters of a real-life AV glove could be changed so as to improve its performance. For example, considering the low frequency range optimal parameter values on the pareto front for k_4 (Set 1 and Set 2), it can be observed that reducing the stiffness of the glove material at the backside of the hand, k_4, will result in a glove that provides better palm transmissibility, but worse finger transmissibility. As a result, a manufacturer may decide to replace the back of a current glove material with a material of lower stiffness so as to increase the effectiveness of the glove in reducing vibrations to the palm. Through observing how glove material properties differ for different Pareto sets, glove manufacturers can select glove materials that enhance or degrade transmissibility at either the palm or finger, depending on their needs.

It should be noted that the optimized AV gloves for the different frequency ranges might be effective provided they are able to meet ergonomic constraints (e.g manual dexterity, percent reduction in grip strength, tool controllability) so as to ensure little to no possibility of injuries as a result of using the gloves.

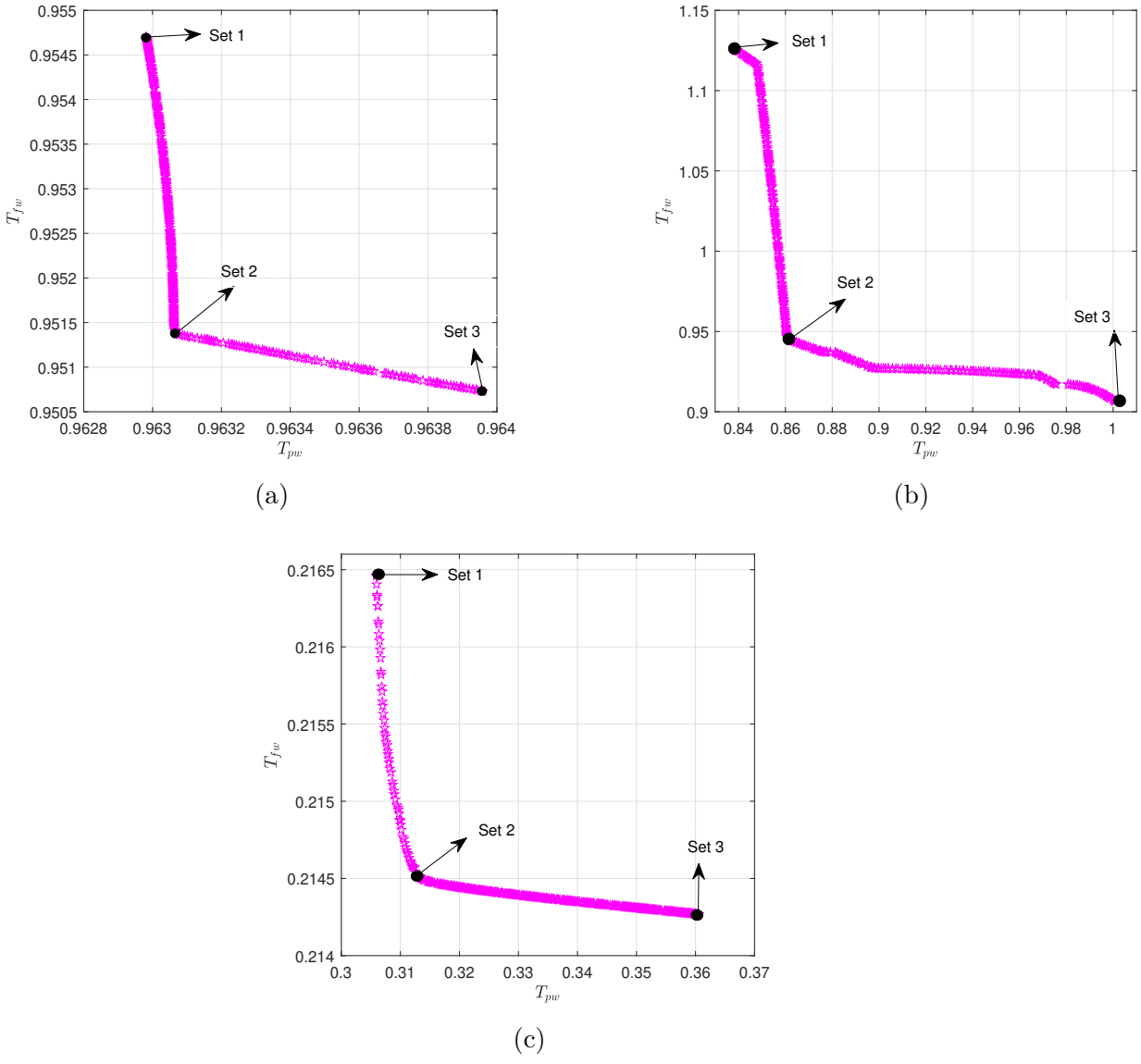

Figure 5.4: Pareto front for (a) low frequency range (b) medium frequency range and c) high frequency range for weighted frequency.

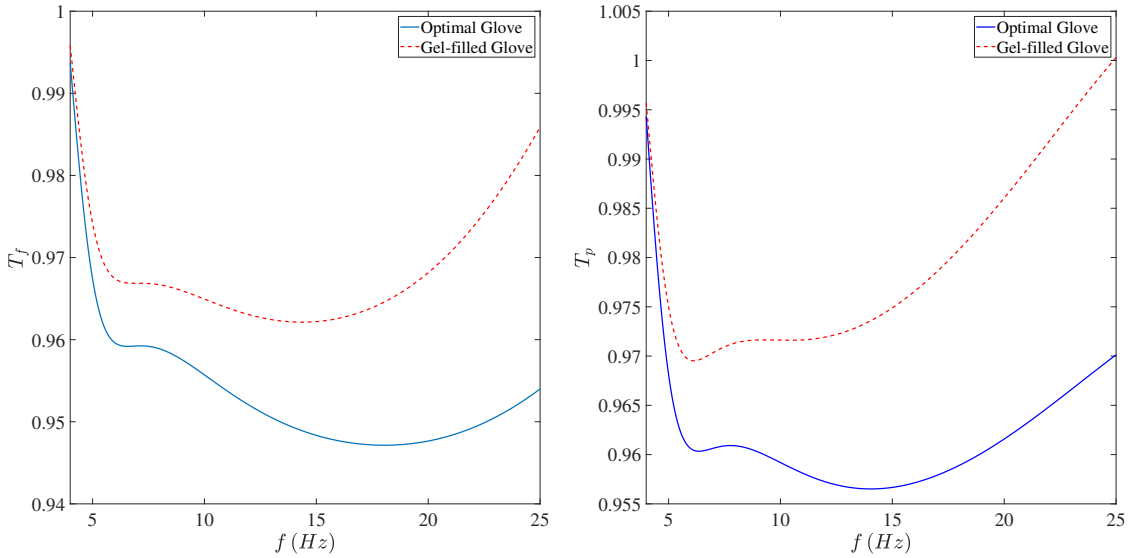

(a) (b)

Figure 5.5: Comparison of relative (a) finger transmissibility (b) palm transmissibility curves for the optimum glove parameters and glove parameters used in Table 4.1. Optimization of the glove parameters is performed for low frequency range.

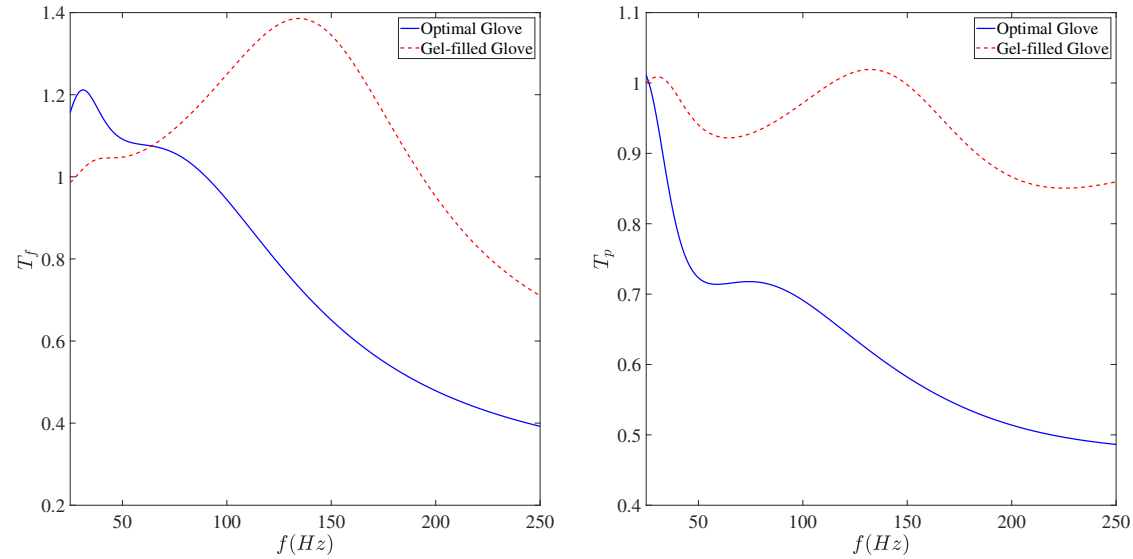

(a) (b)

Figure 5.6: Comparison of relative (a) finger transmissibility (b) palm transmissibility curves for the optimum glove parameters and glove parameters used in Table 4.1. Optimization of the glove parameters is performed for medium frequency range.

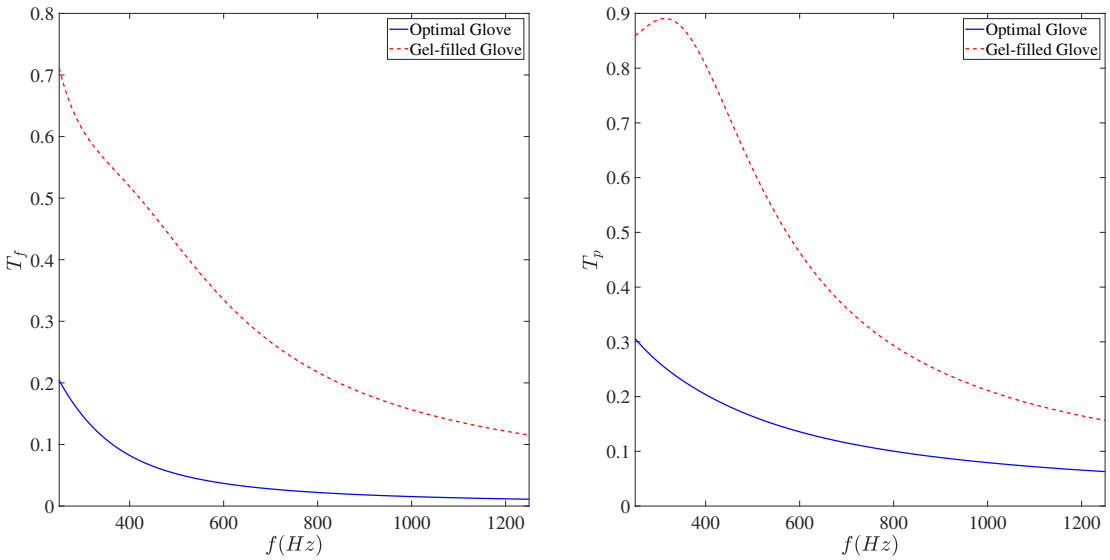

(a) (b)

Figure 5.7: Comparison of relative (a) finger transmissibility (b) palm transmissibility curves for the optimum glove parameters and glove parameters used in Table 4.1. Optimization of the glove parameters is performed for high frequency range.

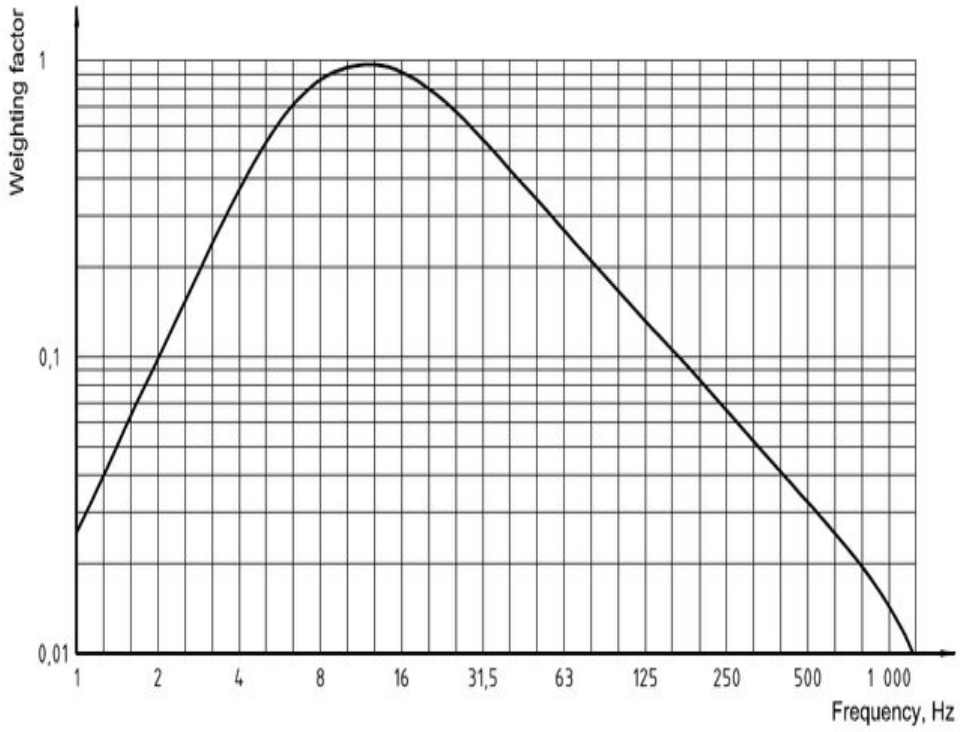

(a)

Figure 5.8: Hand–arm frequency weighting,W_{hi} as defined in ISO 5349-1:2001 [49]

Chapter 6

Conclusion and Future Work

6.1 Conclusion

We studied the vibration of the hand-arm system, using a bio-mechanical lumped parameter model of the system, with and without gloves. For the current analysis, the interaction between different parts of the human hand and hand-tool was considered to be linear for simplicity. These linear interactions were modeled as multiple linear springs and dampers, making the system a multi-degree of freedom system. The closed form solution for the responses of the hand-arm system was obtained using the method of undetermined coefficients. The obtained analytical expressions were validated using direct numerical simulations, and the results showed very good agreement. The effect of different glove parameters on the transmissibility of the palm was investigated with and without a glove.

We discovered that changing the mass and visco-elastic properties of the glove in close contact with the palm or finger masses gave rise to the greatest changes in the relative transmissibility measured at the palm or fingers. Some of these changes included change an increase in the amplitude of the systems resonance peak and also a time shift in the systems resonance peak.

A closer examination of the AV glove system reveals that the system behaves significantly differently when examining how dampening affects the systems response in the palm and

finger amplification and isolation region. The results suggested that the effect of the glove varies based on the frequency range.

Therefore, it was necessary to analyze the glove parameter based on the application and frequency. With this motivation, we optimized the glove parameter for three different frequency ranges to minimize the overall transmissibility using the multi-objective optimization scheme. In each frequency range we obtained optimal values for the AV glove which minimized palm and finger transmissibility. We also observed that for these optimum parameters the transmissibility at most frequencies were minimum as compared to the parameters of a gel-filled AV glove. The implication here is that the AV glove with the parameters defined in the study can be used as a guide by manufacturers to design an anti-vibration glove for different tool applications.

6.2 Future Work

The results of this thesis showed that it is theoretically possible to design an AV glove with optimum parameters that protect the fingers and palm of the hand from vibrations. Towards improving vibration reduction at the steering wheel, the reduction of vibrations transmitted from the steering system using a vibration absorber should also be considered.

In order to reduce the vibrations transmitted from the steering system, a vibration absorber which has been commonly used in hand-tools can be incorporated in a steering wheel system. A schematic of a power tool model with a vibration absorber is shown in Fig 6.3. Rather than using just the AV glove to absorb the brunt of the vibrations, a vibration absorber can also be introduced to absorb vibrations from the steering box of the steering system.

In a study, three different types of absorbers were studied in order to select an absorber which

could best attenuate vibrations from a hand-held power tool [3]. The classic tuned vibration absorber (TVA) was studied as well as a nonlinear tuned vibration absorber (NLTVA) and a nonlinear tuned vibration absorber inerter(NVAI). The spring of the TVA was made nonlinear in order to obtain a NLTVA. An Inerter was then added to the NLTVA to obtain an NVAI.

The study revealed that vibration absorbers were able to significantly reduce the vibration transmitted from the tool to the hand-arm system as depicted in Fig. 6.2a, as compared to when the tool did not have an absorber. Another significant finding from this study was that the NVAI could better reduce vibrations as compared to the TVA and NLTVA when the system begins to operate in a regime where its nonlinearities become apparent (Fig. 6.2b).

This work further motivates us to incorporate absorbers into the steering wheel system to reduce vibrations transmitted to the steering wheel. This work also motivates us to study the steering wheel system and explore operating regions wherein nonlinearities are apparent. If the steering wheel system does exhibit nonlinear behavior, then it will be advantageous to design an absorber which nonlinear properties to best attenuate vibrations of the system.

For the design of vibration absorbers, an increase in the mass of the absorber leads to a better absorber. However, this increase in mass makes the absorber heavier and undesirable in design. To circumvent this issue, inerters that can produce an effective mass more than double their actual mass, have been added to absorber designs [51]. In order to design optimal absorbers for the steering system, absorbers which employ inerters can be explored.

This change will most likely result in less material being needed to design an AV glove that could be used in conjunction with the vibration absorber. This change could also lead to the total elimination of the AV glove depending on how well the vibration absorber is able to reduce vibrations from the steering wheel.

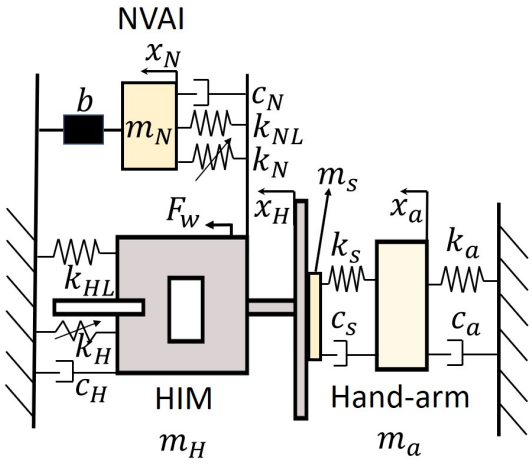

Figure 6.1: Schematic showing model of a hand-held impact machine with a nonlinear absorber-inerter [3].

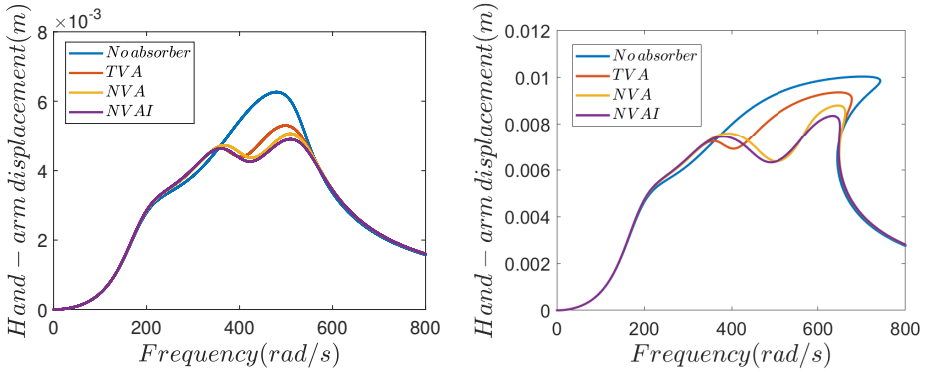

(a) (b)

Figure 6.2: Frequency response of the HAS when coupled to a vibrating equipment containing a linear tuned vibration absorber (TVA), nonlinear tuned vibration absorber(NVA) and a nonlinear tuned vibration absorber-inerter (NVAI). In a) the system is operating in a linear regime and in b) the system response is heavily influenced by its nonlinear characteristic

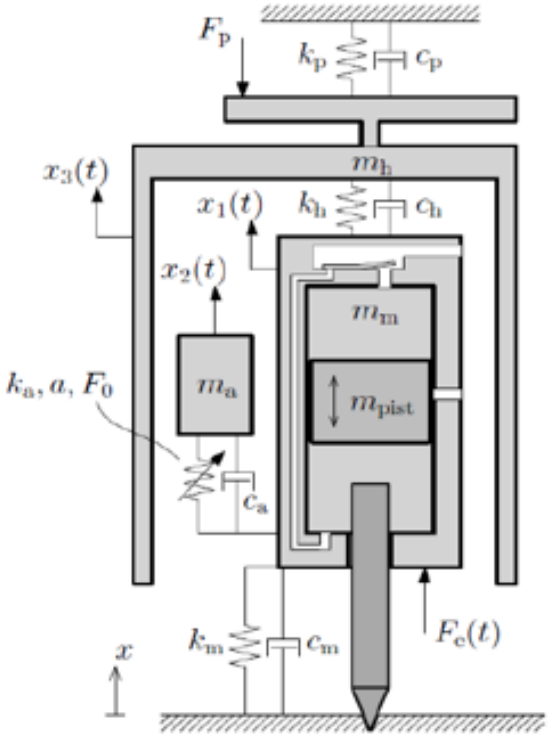

Figure 6.3: Schematic showing incorporation of a vibration absorber in a hand-held power tool [50].

Bibliography

[1] Shamsul Akmar Ab Aziz, Mohd Zaki Nuawi, and Mohd Jailani Mohd Nor. Monitoring of hand-arm vibration. *International Journal of Acoustics & Vibration*, 22(1), 2017.

[2] S Adewusi, S Rakheja, and P Marcotte. Biomechanical models of the human hand-arm to simulate distributed biodynamic responses for different postures. *International Journal of Industrial Ergonomics*, 42(2):249–260, 2012.

[3] Oreoluwa Alabi and Oumar Barry. On the nonlinear vibration analysis of a hand-held impact machine. In *Dynamic Systems and Control Conference*, volume 84287, page V002T29A004. American Society of Mechanical Engineers, 2020.

[4] Jasbir Singh Arora. *Introduction to optimum design*. Elsevier, 2004.

[5] SAA Aziz, MZ Niuawi, MJM Nor, and DDI Daruis. Determination of dominant axis for hand arm vibration (hav) in malaysian army three-tonne truck steering wheels. *Australian Journal of Basic and Applied Sciences*, 8(19):14–16, 2014.

[6] BV Babu and Ashish M Gujarathi. Elitist-multi-objective differential evolution (e-mode) algorithm for multi-objective optimization.

[7] L Barregard, L Ehrenström, and K Marcus. Hand-arm vibration syndrome in swedish car mechanics. *Occupational and environmental medicine*, 60(4):287–294, 2003.

[8] Markus Berger. Understanding antivibration gloves. *Professional Safety*, 62(6):42, 2017.

[9] Bruce P Bernard and Vern Putz-Anderson. Musculoskeletal disorders and workplace factors; a critical review of epidemiologic evidence for work-related musculoskeletal disorders of the neck, upper extremity, and low back. 1997.

[10] Mandal BibhutiB and Srivastava AnupK. Risk from vibration in indian mines. *Indian Journal of Occupational and Environmental Medicine*, 10(2):53–57, 2006.

[11] Chih-Hong Chang, Mao-Jiun J Wang, and Shu-Chiang Lin. Evaluating the effects of wearing gloves and wrist support on hand–arm response while operating an in-line pneumatic screwdriver. *International Journal of Industrial Ergonomics*, 24(5):473–481, 1999.

[12] David D Chase and Daniel A Talonn. Vibration attenuating member and method of making same, October 7 1997. US Patent 5,673,437.

[13] T Cherian, S Rakheja, and RB Bhat. An analytical investigation of an energy flow divider to attenuate hand-transmitted vibration. *International Journal of Industrial Ergonomics*, 17(6):455–467, 1996.

[14] Eric Courteille, Frédéric Mortier, Lionel Leotoing, and Eric Ragneau. Multi-objective robust design optimization of an engine mounting system. Technical report, SAE Technical Paper, 2005.

[15] KN Dewangan and VK Tewari. Characteristics of hand-transmitted vibration of a hand tractor used in three operational modes. *International journal of industrial ergonomics*, 39(1):239–245, 2009.

[16] Jennie H Dong, Ren G Dong, Subhash Rakheja, Daniel E Welcome, Thomas W McDowell, and John Z Wu. A method for analyzing absorbed power distribution in the hand and arm substructures when operating vibrating tools. *Journal of Sound and Vibration*, 311(3-5):1286–1304, 2008.

[17] Ren G Dong, Thomas W McDOWELL, and Daniel E Welcome. Biodynamic response

at the palm of the human hand subjected to a random vibration. *Industrial Health*, 43 (1):241–255, 2005.

[18] Ren G Dong, John Z Wu, and Daniel E Welcome. Recent advances in biodynamics of human hand-arm system. *Industrial health*, 43(3):449–471, 2005.

[19] Ren G Dong, Jennie H Dong, John Z Wu, and Subhash Rakheja. Modeling of biodynamic responses distributed at the fingers and the palm of the human hand–arm system. *Journal of Biomechanics*, 40(10):2335–2340, 2007.

[20] Ren G Dong, Thomas W McDowell, Daniel E Welcome, Christopher Warren, John Z Wu, and Subhash Rakheja. Analysis of anti-vibration gloves mechanism and evaluation methods. *Journal of Sound and Vibration*, 321(1-2):435–453, 2009.

[21] Ren G Dong, Daniel E Welcome, Xueyan S Xu, Christopher Warren, Thomas W McDowell, John Z Wu, and Subhash Rakheja. Mechanical impedances distributed at the fingers and palm of the human hand in three orthogonal directions. *Journal of Sound and Vibration*, 331(5):1191–1206, 2012.

[22] RG Dong, TW McDowell, DE Welcome, WP Smutz, AW Schopper, C Warren, JZ Wu, and S Rakheja. On-the-hand measurement methods for assessing effectiveness of anti-vibration gloves. *International Journal of Industrial Ergonomics*, 32(4):283–298, 2003.

[23] RG Dong, S Rakheja, TW McDowell, DE Welcome, JZ Wu, C Warren, J Barkley, B Washington, and AW Schopper. A method for assessing the effectiveness of anti-vibration gloves using biodynamic responses of the hand–arm system. *Journal of Sound and Vibration*, 282(3-5):1101–1118, 2005.

[24] Sonja Falkiner. Diagnosis and treatment of hand-arm vibration syndrome and its relationship to carpal tunnel syndrome. *Australian family physician*, 32(7), 2003.

[25] International Organization for Standardization (ISO). Iso 10819: 2013 mechanical vibration and shock; hand-arm vibration: Measurement and evaluation of the vibration transmissibility of gloves at the palm of the hand, 2013.

[26] Mary K Freund, Farzaneh Joubaneh, Oumar R Barry, Emad Y Tanbour, et al. Study of vibration of electric power steering systems using a continuous system model. In *ASME 2017 International Mechanical Engineering Congress and Exposition*. American Society of Mechanical Engineers Digital Collection, 2017.

[27] Martin Fritz. An improved biomechanical model for simulating the strain of the hand-arm system under vibration stress. *Journal of biomechanics*, 24(12):1165–1171, 1991.

[28] G Gemne and W Taylor. Foreword: Hand-arm vibration and the central autonomic nervous system. *Journal of Low Frequency Noise and Vibration*, 2:1–12, 1983.

[29] J Giacomin and F Fustes. Subjective equivalence of steering wheel vibration and sound. *International Journal of Industrial Ergonomics*, 35(6):517–526, 2005.

[30] VIJAY K GOEL and Kwan Rim. Role of gloves in reducing vibration: An analysis for pneumatic chipping hammer. *American Industrial Hygiene Association Journal*, 48(1): 9–14, 1987.

[31] Vlado Goglia, Zlatko Gospodarić, Silvio Košutić, and Danka Filipović. Hand-transmitted vibration from the steering wheel to drivers of a small four-wheel drive tractor. *Applied ergonomics*, 34(1):45–49, 2003.

[32] Vlado Goglia, Zlatko Gospodaric, Dubravko Filipovic, and Igor Djukic. Influence on operator's health of hand-transmitted vibrations from handles of a single-axle tractor. *Annals of agricultural and environmental medicine*, 13(1):33, 2006.

[33] Michael J Griffin et al. Foundations of hand-transmitted vibration standards. *Nagoya J Med Sci*, 57(Suppl):147–164, 1994.

[34] MJ Griffin, CR Macfarlane, and CD Norman. The transmission of vibration to the hand and the influence of gloves. In *Vibration Effects on the Hand and Arm in Industry*, pages 103–116. Wiley, New York, 1982.

[35] MJ Griffin, M Bovenzi, and CM Nelson. Dose-response patterns for vibration-induced white finger. *Occupational and Environmental Medicine*, 60(1):16–26, 2003.

[36] R Gurram, S Rakheja, and GJ Gouw. Mechanical impedance of the human hand-arm system subject to sinusoidal and stochastic excitations. *International Journal of Industrial Ergonomics*, 16(2):135–145, 1995.

[37] R Gurram, S Rakheja, PE Boileau, and GJ Gouw. Development of a grip force dependent hand-arm vibration model. *Central European journal of public health*, 4(1):65–68, 1996.

[38] Mats Hagberg. Clinical assessment of musculoskeletal disorders in workers exposed to hand-arm vibration. *International archives of occupational and environmental health*, 75(1):97–105, 2002.

[39] K Hamouda, S Rakheja, KN Dewangan, and P Marcotte. Fingers' vibration transmission and grip strength preservation performance of vibration reducing gloves. *Applied ergonomics*, 66:121–138, 2018.

[40] Karim Hamouda, Subhash Rakheja, Pierre Marcotte, and KN Dewangan. Fingers vibration transmission performance of vibration reducing gloves. *International Journal of Industrial Ergonomics*, 62:55–69, 2017.

[41] Ko Ying Hao, Lee Xin Mei, and Zaidi Mohd Ripin. Tuned vibration absorber for suppression of hand-arm vibration in electric grass trimmer. *International journal of industrial ergonomics*, 41(5):494–508, 2011.

[42] N Harada and MH Mahbub. Diagnosis of vascular injuries caused by hand-transmitted vibration. *International archives of occupational and environmental health*, 81(5):507–518, 2008.

[43] C Heaver, KS Goonetilleke, H Ferguson, and S Shiralkar. Hand–arm vibration syndrome: a common occupational hazard in industrialized countries. *Journal of Hand Surgery (European Volume)*, 36(5):354–363, 2011.

[44] S Hewitt. Triaxial measurements of the performance of anti-vibration gloves. *HSE research report RR795*, 2010.

[45] Sue Hewitt, Ren Dong, Tom McDowell, and Daniel Welcome. The efficacy of anti-vibration gloves. *Acoustics Australia*, 44(1):121–127, 2016.

[46] Yoshio TOM INAGA. The relationship between vibration exposure and symptoms of vibration syndrome. 1993.

[47] Daniel J Inman and Ramesh Chandra Singh. *Engineering vibration*, volume 3. Prentice Hall Englewood Cliffs, NJ, 1994.

[48] EN ISO. 10819 (1996) mechanical vibration and shock—hand-arm vibration—method for the measurement and evaluation of the vibration transmissibility of gloves at the palm of the hand. *European Committee for Standardization, Brussels*, 2000.

[49] ISO ISO. 5349-1: Mechanical vibration—measurement and evaluation of human exposure to hand-transmitted vibration—part 1: general requirements. *Geneva, Switzerland: International Organization for Standardization*, 2001.

[50] Mattias Josefsson and Snævar Leó Grétarsson. Optimisation of a non-linear tuned vibration absorber in a hand-held impact machine. Master's thesis, 2015.

[51] Eshagh Farzaneh Joubaneh and Oumar Rafiou Barry. On the improvement of vibration mitigation and energy harvesting using electromagnetic vibration absorber-inerter: Exact h2 optimization. *Journal of Vibration and Acoustics*, 141(6):061007, 2019.

[52] Van Quynh Le and Khac Tuan Nguyen. Optimal design parameters of cab's isolation system for vibratory roller using a multi-objective genetic algorithm. In *Applied Mechanics and Materials*, volume 875, pages 105–112. Trans Tech Publ, 2018.

[53] Deukpyo Lee, Yun Gab Lo, Minwoo Han, Kyuwon Kim, and Chulhee Kim. A development of the model based torque feedback control with disturbance observer for electric power steering system. Technical report, SAE Technical Paper, 2019.

[54] Xin Li, XP Zhao, and Jie Chen. Sliding mode control for torque ripple reduction of an electric power steering system based on a reference model. *Proceedings of the Institution of Mechanical Engineers, Part D: Journal of Automobile Engineering*, 222 (12):2283–2290, 2008.

[55] Xin Li, Xue-Ping Zhao, and Jie Chen. Controller design for electric power steering system using ts fuzzy model approach. *International Journal of Automation and Computing*, 6(2):198–203, 2009.

[56] Yijun Li, Taehyun Shim, Dexin Wang, and Timothy Offerle. Investigation of factors affecting steering feel of column assist electric power steering. In *ASME 2016 Dynamic Systems and Control Conference*. American Society of Mechanical Engineers Digital Collection, 2016.

[57] Qingfeng Liu, Qifeng Wu, Zifang Zeng, Lihua Xia, and Yong Huang. Clinical effect

and mechanism of acupuncture and moxibustion on occupational hand-arm vibration disease: A retrospective study. *European Journal of Integrative Medicine*, 23:109–115, 2018.

[58] Bibhuti B Mandal and Anup K Srivastava. Risk from vibration in indian mines. *Indian Journal of Occupational and Environmental Medicine*, 10(2):53, 2006.

[59] Giuseppe Carlo Marano, Giuseppe Quaranta, and Rita Greco. Multi-objective optimization by genetic algorithm of structural systems subject to random vibrations. *Structural and Multidisciplinary Optimization*, 39(4):385–399, 2009.

[60] Thomas W McDowell, Ren G Dong, Daniel E Welcome, Xueyan S Xu, and Christopher Warren. Vibration-reducing gloves: transmissibility at the palm of the hand in three orthogonal directions. *Ergonomics*, 56(12):1823–1840, 2013.

[61] Khairil Anas Md Rezali and Michael J Griffin. Transmission of vibration through gloves: effects of material thickness. *Ergonomics*, 59(8):1026–1037, 2016.

[62] Nader Nariman-Zadeh, M Salehpour, Ali Jamali, and E Haghgoo. Pareto optimization of a five-degree of freedom vehicle vibration model using a multi-objective uniform-diversity genetic algorithm (muga). *Engineering Applications of Artificial Intelligence*, 23(4):543–551, 2010.

[63] Lars E Necking, Göran Lundborg, Ronnie Lundström, Lars-Eric Thornell, and Jan Fridén. Hand muscle pathology after long-term vibration exposure. *Journal of Hand Surgery*, 29(5):431–437, 2004.

[64] Busi Nyantumbu, Chris M Barber, Mary Ross, Andrew D Curran, David Fishwick, Belinda Dias, Spo Kgalamono, and James I Phillips. Hand–arm vibration syndrome in south african gold miners. *Occupational Medicine*, 57(1):25–29, 2007.

[65] GS Paddan and MJ Griffin. Measurement of glove and hand dynamics using knuckle vibration. In *Proceedings of the 9th International Conference on Hand-arm Vibration, Section*, volume 15, 2001.

[66] Peter L Pelmear and William Taylor. *Hand-arm vibration: A comprehensive guide for occupational health professionals*. Van Nostrand Reinhold Company, 1992.

[67] I Pinto, N Stacchini, Massimo Bovenzi, GS Paddan, and MJ Griffin. Protection effectiveness of anti-vibration gloves: field evaluation and laboratory performance assessment. In *Proceedings of the 9th International Conference on Hand-arm Vibration*, pages 387–96, 2001.

[68] Ilmari Pyykkö, Markus Färkkilä, Jarmo Toivanen, Olli Korhonen, and Juhani Hyvärinen. Transmission of vibration in the hand-arm system with special reference to changes in compression force and acceleration. *Scandinavian Journal of Work, Environment & Health*, pages 87–95, 1976.

[69] S Rakheja, R Gurram, and GJ Gouw. Development of linear and nonlinear hand-arm vibration models using optimization and linearization techniques. *Journal of biomechanics*, 26(10):1253–1260, 1993.

[70] S Rakheja, JZ Wu, RG Dong, AW Schopper, and P-É Boileau. A comparison of biodynamic models of the human hand–arm system for applications to hand-held power tools. *Journal of Sound and Vibration*, 249(1):55–82, 2002.

[71] D Reynolds, D Weaver, and T Jetzer. Application of a new technology to the design of effective anti-vibration gloves. *Central european journal of public health*, 4(2):140–144, 1996.

[72] DD Reynolds and EN Angevine. Hand-arm vibration, part ii: Vibration transmission

characteristics of the hand and arm. *Journal of sound and vibration*, 51(2):255–265, 1977.

[73] Md Rezali, Khairil Anas, and Michael J Griffin. The transmission of vibration through gloves to the hand and to the fingers: Effects of material dynamic stiffness. In *Applied Mechanics and Materials*, volume 564, pages 149–154. Trans Tech Publ, 2014.

[74] Ananth Sakthivel, Sethuraman Sriraman, and Rakesh B Verma. Study of vibration from steering wheel of an agricultural tractor. *SAE International Journal of Commercial Vehicles*, 5(2012-01-1908):441–454, 2012.

[75] Elsjebe Sampson and Johannes L Van Niekerk. Literature survey on anti-vibration gloves. 2003.

[76] Trygve Strömberg, Lars B Dahlin, Arne Brun, and Goran Lundborg. Structural nerve changes at wrist level in workers exposed to vibration. *Occupational and environmental medicine*, 54(5):307–311, 1997.

[77] Ying Sun, Ping He, Yunqing Zhang, and Liping Chen. Modeling and co-simulation of hydraulic power steering system. In *2011 third international conference on measuring technology and mechatronics automation*, volume 2, pages 595–600. IEEE, 2011.

[78] VK Tewari and KN Dewangan. Effect of vibration isolators in reduction of work stress during field operation of hand tractor. *Biosystems Engineering*, 103(2):146–158, 2009.

[79] Per Vihlborg, Liss Bryngelsson, Bernt Lindgren, Lars Gunnar Gunnarsson, and Pål Graff. Association between vibration exposure and hand-arm vibration symptoms in a swedish mechanical industry. *International Journal of Industrial Ergonomics*, 62:77–81, 2017.

[80] Donald W Wasserman. Occupational vibration: Are you at risk. *Quest Technologies special report. Quest Technologies: Oconomowoc, WI*, 53066:2, 2005.

[81] Huang Wei, Jian Xu, Da-yong Zhu, Ying-lei Wu, Jian-wei Lu, and Kun-lin Lu. Multi-objective optimization of parameters and location of passive vibration isolation system excited by clamped thin plate foundation. *Engineering Review: Međunarodni časopis namijenjen publiciranju originalnih istraživanja s aspekta analize konstrukcija, materijala i novih tehnologija u području strojarstva, brodogradnje, temeljnih tehničkih znanosti, elektrotehnike, računarstva i građevinarstva*, 36(1):19–27, 2016.

[82] Daniel E Welcome, Ren G Dong, Xueyan S Xu, Christopher Warren, and Thomas W McDowell. The effects of vibration-reducing gloves on finger vibration. *International journal of industrial ergonomics*, 44(1):45–59, 2014.

[83] Bryan Wimer, Thomas W McDowell, Xueyan S Xu, Daniel E Welcome, Christopher Warren, and Ren G Dong. Effects of gloves on the total grip strength applied to cylindrical handles. *International Journal of Industrial Ergonomics*, 40(5):574–583, 2010.

[84] JZ Wu, K Krajnak, DE Welcome, and RG Dong. Analysis of the dynamic strains in a fingertip exposed to vibrations: Correlation to the mechanical stimuli on mechanoreceptors. *Journal of biomechanics*, 39(13):2445–2456, 2006.

[85] Qianfan Xin. *Diesel engine system design*. Elsevier, 2011.

[86] Yumeng Yao, Subhash Rakheja, Chantal Gauvin, Pierre Marcotte, and Karim Hamouda. Evaluation of effects of anti-vibration gloves on manual dexterity. *Ergonomics*, pages 1–15, 2018.

[87] Wan-Suk Yoo, Sang-Do Na, and Min-Seok Kim. Relationship between subjective and

objective evaluations of steering wheel vibration. *Journal of mechanical science and technology*, 25(7):1695, 2011.

[88] Lofti Zadeh. Optimality and non-scalar-valued performance criteria. *IEEE transactions on Automatic Control*, 8(1):59–60, 1963.

[89] Md Zakaullah Zaka, Mohd Saad Saleem, Abdul Khaliq, and Mohd Afzal. Effect of hand transmitted vibration through tractor during ploughing field. *International Journal of Engineering Research and Applications*, 4(12):18–23, 2014.

[90] Barbara Zardin, Massimo Borghi, Francesco Gherardini, and Nicholas Zanasi. Modelling and simulation of a hydrostatic steering system for agricultural tractors. *Energies*, 11 (1):230, 2018.

[91] Nong Zhang and Miao Wang. Dynamic modeling of hydraulic power steering system with variable ratio rack and pinion gear. *JSME International Journal Series C Mechanical Systems, Machine Elements and Manufacturing*, 48(2):251–260, 2005.

[92] Walter Zottin, Ana Paula Curty Cuco, Marcus Vinícius F dos Reis, and Rodrigo Ferraz AF da Silva. Application of optimization techniques in the design of engine components. Technical report, SAE Technical Paper, 2008.

Appendices

Appendix A

Expressions used in Eqs. (3.5) and Eqs. (3.10)

$$[\mathbf{M}] = \begin{bmatrix} m_0 & 0 & 0 & 0 \\ 0 & m_f & 0 & 0 \\ 0 & 0 & m_p & 0 \\ 0 & 0 & 0 & m_{tf} + m_{tp} + m_H \end{bmatrix}$$

$$[\mathbf{C}] = \begin{bmatrix} c_0 + c_w & 0 & -c_w & 0 \\ 0 & c_1 + c_2 & -c_1 & -c_2 \\ -c_w & -c_1 & c_w + c_1 + c_3 & -c_3 \\ 0 & -c_2 & -c_3 & c_2 + c_3 + c_s \end{bmatrix}$$

$$[\mathbf{K}] = \begin{bmatrix} k_0 + k_w & 0 & -k_w & 0 \\ 0 & k_1 + k_2 & -k_1 & -k_2 \\ -k_w & -k_1 & k_w + k_1 + k_3 & -k_3 \\ 0 & -k_2 & -k_3 & k_2 + k_3 + k_s \end{bmatrix}$$

$$[\mathbf{F_{eq}}] = \begin{bmatrix} 0 \\ 0 \\ 0 \\ c_s\dot{z} + k_s z \end{bmatrix}$$

$$[\hat{\mathbf{F}}_{\mathbf{eq}}] = \begin{bmatrix} 0 \\ 0 \\ 0 \\ 0 \\ 0 \\ c_s\dot{z} + k_s z \end{bmatrix}$$

$$[\mathbf{M_1}] = \begin{bmatrix} m_0 & 0 & 0 & 0 & 0 & 0 \\ 0 & m_f + m_{g1} & 0 & 0 & 0 & 0 \\ 0 & 0 & m_p + m_{g2} & 0 & 0 & 0 \\ 0 & 0 & 0 & m_{tp} + m_{g4} & 0 & 0 \\ 0 & 0 & 0 & 0 & m_{tf} + m_{g3} & 0 \\ 0 & 0 & 0 & 0 & 0 & m_{g5} + m_{g6} + m_H \end{bmatrix}$$

$$[\mathbf{C_1}] = \begin{bmatrix} \mathbf{C1} & \mathbf{C2} \\ \mathbf{C2^T} & \mathbf{C3} \end{bmatrix}$$

$$[\mathbf{C1}] = \begin{bmatrix} c_0 + c_w & 0 & -c_w \\ 0 & c_1 + c_4 + c_2 & -c_1 - c_4 \\ -c_w & -c_1 - c_4 & c_1 + c_4 + c_3 + c_w \end{bmatrix}$$

$$[\mathbf{C2}] = \begin{bmatrix} 0 & 0 & 0 \\ 0 & -c_2 & 0 \\ -c_3 & 0 & 0 \end{bmatrix}$$

$$[\mathbf{C3}] = \begin{bmatrix} c_3 + c_5 + c_7 & -c_5 & -c_7 \\ -c_5 & c_2 + c_5 + c_6 & -c_6 \\ -c_7 & -c_6 & c_6 + c_7 + c_s \end{bmatrix}$$

$$[\mathbf{K_1}] = \begin{bmatrix} \mathbf{K1} & \mathbf{K2} \\ \mathbf{K2^T} & \mathbf{K3} \end{bmatrix}$$

$$[\mathbf{K1}] = \begin{bmatrix} k_0 + k_w & 0 & -k_w \\ 0 & k_1 + k_4 + k_2 & -k_1 - k_4 \\ -k_w & -k_1 - k_4 & k_1 + k_4 + k_3 + k_w \end{bmatrix}$$

$$[\mathbf{K2}] = \begin{bmatrix} 0 & 0 & 0 \\ 0 & -k_2 & 0 \\ -k_3 & 0 & 0 \end{bmatrix}$$

$$[\mathbf{K3}] = \begin{bmatrix} k_3 + k_5 + k_7 & -k_5 & -k_7 \\ -k_5 & k_2 + k_5 + k_6 & -k_6 \\ -k_7 & -k_6 & k_6 + k_7 + k_s \end{bmatrix}$$